ANALYSIS AND SYNTHESIS OF A LINEAR, SELF ADAPTIVE, STABILITY AUGMENTATION SYSTEM

Marcel Dandois **Convair**

In the operational concepts for many new high-speed high-altitude aircraft and missiles, extreme variations in flight environment are required. As a result of these requirements, designers of aircraft control systems have had difficulties in arriving at system concepts through whose implementation uniform response and stability characteristics could be obtained at all flight conditions. In recent higher performance airplanes, uniform stability has been obtained by scheduling control parameters as functions of air data measurements. Use of this approach has led to the requirement that the aircraft carry a reliable, accurate air data computer. It has also led to the requirement that the dynamic stability of the aircraft be predictable at all flight conditions so that the proper control compensations may be scheduled.

Difficulties in providing these capabilities have led to the use of a different approach. In this approach uniform stability is obtained by compensating for changes in aircraft stability directly. This may be accomplished by adjusting control parameters as functions of the airframe response or by other special arrangements (with fixed parameters) that maintain a uniform response over a wide range of conditions. Control systems falling in this category have been called "Self-Adaptive Controls."

The need for self-adaptive flight control systems for applications to military aircraft was brought to the attention of the aircraft industry at WADC in the fall of 1955. As a result of activities undertaken at WADC and sponsored by this agency and as a result of independent research work in advanced automatic control systems already under way at other agencies, Convair embarked on a company-sponsored study and survey of self-adaptive methods of control. From a review of the available literature related to this subject and from original studies made at Convair, there emerged several methods of control which merited preliminary investigation. These techniques have been described in Reference 1.

Upon completion of this preliminary survey, this corporate program was extended in the form of a more detailed study of one of these techniques. It was felt that, in order to be worthwhile, the control method selected should provide a sizeable improvement in stability augmentation over presently employed control systems and should allow the incorporation of the method in present systems with little redesign. For these reasons, a method was selected which

comprised a control system made up of three linear feedback loops with fixed parameters. These consisted of position, rate, and acceleration feedback whose combined dynamic effects represent the inverse of the desired system dynamics. With sufficient control gain this arrangement results in a system which maintains desired aircraft characteristics over a wide range of conditions. The higher the gain, the more insensitive the system becomes to changes in flight environment. Although well known in servo theory, this method has not been generally applied to flight control systems because of the likelihood of encountered instability as a result of the high feedback gains. It can be shown that this tendency is due essentially to the dynamic effects of the sensors and servo actuator characteristics. With the advent of control instrumentation with superior response rates, higher gains will be allowable, and this method may become practical in certain applications. Because of its simplicity, it appears worthwhile to investigate the advantages and limitations of this method in a typical application. Results of this investigation are presented in the present report.

There are some methods of self-adaptive control which, by means of simplifying assumptions, may be linearized to a special arrangement of high gain feedback. Simplifications such as these entail a loss in the representation of the original system and are justifiable only as methods of obtaining the distinguishing characteristics to be expected.

The particular method which is discussed in this report may be viewed in fact as a simplification of a self-adaptive control in which a measurement of damping ratio is employed to adjust the feedback parameters. Therefore, the results herein also show the approximate performance to be expected, within certain restrictions, with a type of nonlinear self-adaptive control.

NOTATION

$A(s)$	Term in the denominator of closed-loop transfer function of airplane-control system
$B(s)$	Term in the denominator of closed-loop transfer function of airplane-control system
C	Selected value of measured short period undamped natural frequency
C_1	Steady state gain of hydraulic actuator
C_2	Gain of feedback loop around hydraulic actuator
C_3	Steady state gain of rate gyro
f_r	Viscous damping of rate gyro output axis
$F_o(s)$	Numerator of closed-loop transfer function of typical controlled system
$G_o(s)$	Desired transfer function of typical system
H	Spin momentum of rate gyro
$H(s)$	Transfer function of feedback elements in typical control system
I	Moment of inertia of accelerometer mass
J_r	Moment of inertia of rate gyro about the free axis
k	Torsional spring constant of angular accelerometer
K	Arbitrary multiplying factor
K_i	Elastic constant of rate gyro input axis
K_r	Elastic constant of rate gyro output axis
K_o	Airframe steady state gain
K_1	Design closed-loop steady state gain of airframe-control system
K_2	Variable loop gain in airframe-control system

NOTATION (Cont'd)

K_{2a}	Portion of variable loop gain in forward loop of airframe-control system
K_{2b}	Portion of variable loop gain in feedback loop of airframe-control system
K_3	Actual closed-loop steady state gain of airframe-control system
K_4	Adjustable feedback gain which determines amount of damping ratio control
P(s)	Term in open-loop transform of typical system
Q(s)	Term in open-loop transform of typical system
s	Laplace transform complex variable
x(s)	Transform of input to servo actuator
$\delta_e(s)$	Laplace transform of elevator deflection
ζ_A	Accelerometer damping ratio
ζ_m	Measured airplane short period damping ratio
ζ_q	Damping ratio of second order lead term in approximation of B(s)
ζ_x	Damping ratio of hydraulic actuator second order lag factor
ζ_0	Free airframe short period damping ratio
ζ_1	Design airframe short period damping ratio
ζ_3	Actual closed-loop damping ratio of airframe-control system
ζ'	Quasi damping ratio of closed-loop airframe-control system
$\theta_C(s)$	Input command to airframe pitch control system
$\theta_0(s)$	Laplace transform of airframe output pitch deflection

NOTATION (Cont'd)

$\dot{\theta}_{0_m}$	Angular deflection of rate gyro output
$\ddot{\theta}_{0_m}$	Angular deflection of accelerometer mass with respect to accelerometer case
ω_A	Accelerometer undamped natural frequency
ω_{HS}	Hydraulic servo characteristic frequency
ω_i	Frequency at intersection of dual Nyquist diagram
ω_m	Measured airplane short period undamped natural frequency
ω_p	Characteristic frequency of first order lead term in approximation of B(s)
ω_q	Undamped natural frequency of second order lead term in approximation of B(s)
ω_{RG_1}	Characteristic frequency of rate gyro first order factor
ω_{RG_2}	Characteristic frequency of rate gyro first order factor
ω_{RG}	Rate gyro characteristic frequency
ω_x	Undamped natural frequency of hydraulic actuator second order lag factor
ω_0	Free airframe short period undamped natural frequency
ω_1	Design airframe short period undamped natural frequency
ω_3	Actual closed-loop undamped natural frequency of airframe-control system
ω_I, ω_{II}, ω_{III}, ω_{IV}	frequencies on dual Nyquist diagram.

DESCRIPTION OF METHOD

The control system discussed in this report consists of a feedback configuration whose transfer function is equivalent to the reciprocal of the desired aircraft characteristics. The method also may be regarded as a simplified version of a self-adaptive control in which a measurement of damping ratio is employed to adjust its feedback parameters. These two concepts will be explained in detail.

Reciprocal Model Feedback Concept

The first concept is not new. It stems from an elementary principle of feedback control which may be illustrated as follows. Let $G_o(s)$ be the transfer function of a system whose response characteristics are to be controlled. Assume that this function varies with environmental operating conditions. Let $G_1(s)$ be a fixed transfer function representing desired dynamic characteristics of $G_o(s)$. In the following block diagram a feedback configuration is shown which forces the dynamic characteristics of the system to approach the desired values regardless of changes in $G_o(s)$.

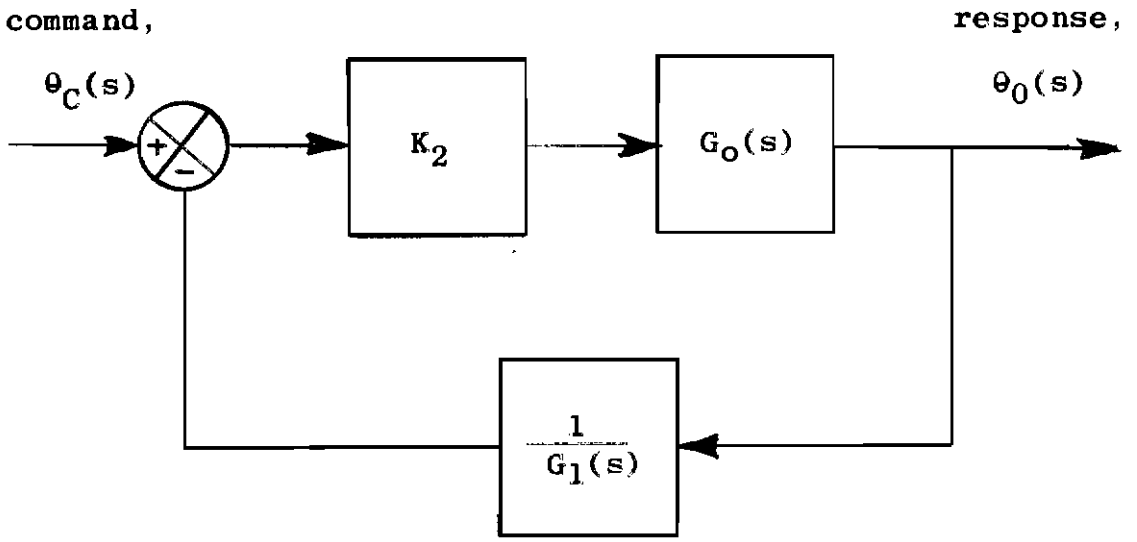

Fig. 1 - ILLUSTRATION OF FEEDBACK COMPENSATION

The function $\frac{1}{G_1(s)}$ is the transfer function of elements of the feedback path, $\theta_0(s)$ is the output response transform, and $\theta_C(s)$ is the input command transform. The factor K_2 represents a variable gain term which is introduced to allow the proper degree of feedback correction to be applied.

The magnitude which K must assume in order to force the transfer function of the closed system to approach $G_1(s)$ are dictated by the formula given below, which expresses the closed loop transfer function:

$$\frac{\theta_0(s)}{\theta_C(s)} = \frac{K_2G(s)}{1 + \frac{K_2G(s)}{G_1(s)}} \qquad (1)$$

It is evident from Equation 1 that if the gain K_2 is made sufficiently large so that

$$\left| \frac{K_2G_o(s)}{G_1(s)} \right| \gg 1 \qquad (2)$$

then the transfer function is reduced to

$$\frac{\theta_0(s)}{\theta_C(s)} \approx G_1(s). \qquad (3)$$

The condition which must be satisfied is

$$K_2 \gg \left| \frac{G_1(s)}{G_o(s)} \right| . \qquad (4)$$

It is to be noted that $G_1(s)$ is independent of the airframe transfer function. The magnitude of K_2 is dictated by Equation 4; it is affected by variations in the airframe characteristics $|G_o(s)|$. The larger K_2 becomes, the smaller is the effect of $|G_o(s)|$ and the larger are the tolerable variations in $|G_o(s)|$. The terms $|G_o(s)|$ and $|G_1(s)|$ are frequency dependent functions; therefore, the choice of K_2 is affected by the range of frequency within which best control is required.

The method described above may be used in airplane and missile flight control systems to improve the stability of their natural modes of motion and to maintain a specified stability regardless of flight condition. An example is illustrated in Figure 2a in which the longitudinal short period motion is augmented by means of a feedback loop having characteristics equal to the reciprocal of the desired short period motion. The transfer function expressing this motion in response to a commanded elevator deflection (or any suitable longitudinal control surface) may be expressed as follows:

$$\frac{\theta_0(s)}{\theta_C(s)} = \frac{K_o}{\frac{s2}{\omega_0^2} + \frac{2\zeta_0 s}{\omega_0} + 1} \cdot \quad (5)$$

The term K_o represents the steady state pitch sensitivity to elevator commands. The natural frequency and damping ratio is specified by ω_0 and ζ_0, respectively. These terms vary with flight conditions.

The feedback terms shown in Figure 2a are equivalent to the reciprocal of the transfer function in Equation 5 except that fixed optimum values are chosen for the steady state gain, the natural frequency, and the damping ratio.

Synthesis of the feedback function may be accomplished by sensing pitch attitude, pitch rate, and pitch acceleration, multiplying each by the appropriate gain, and by summing the results. This is shown in Figure 2b.

Damping Ratio Feedback Concept

The feedback system illustrated in Figure 2b may be synthesized on the basis of a different control cencept. The basic method of synthesis is illustrated in Figure 3a. The system shown consists of rate feedback divided into two parts, one with a fixed gain and one with a variable gain adjusted as a function of measured damping ratio, ζ_m. Since an increase in pitch rate negative feedback causes an increase in pitch damping, it is obvious that the gain multiplying factor ζ_m must be introduced in such a manner that a decrease in the over-all negative feedback is attained when damping increases. In Figure 3a the factor ζ_m multiplies a portion of the rate feedback signal determined by K_4, and this portion is then applied as the positive feedback shown by the minus sign at the summing point. Since positive feedback has an effect opposite to

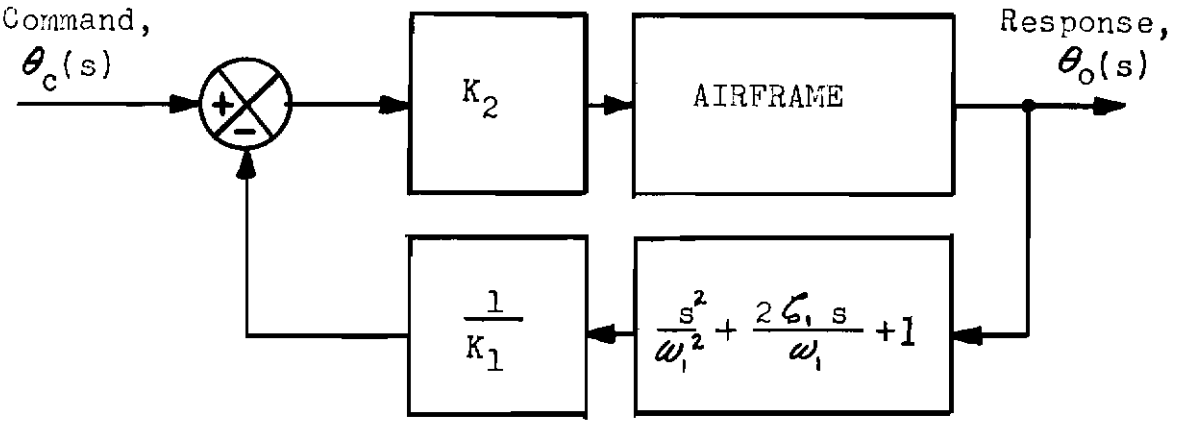

Fig. 2a SHORT PERIOD CONTROL CONFIGURATION

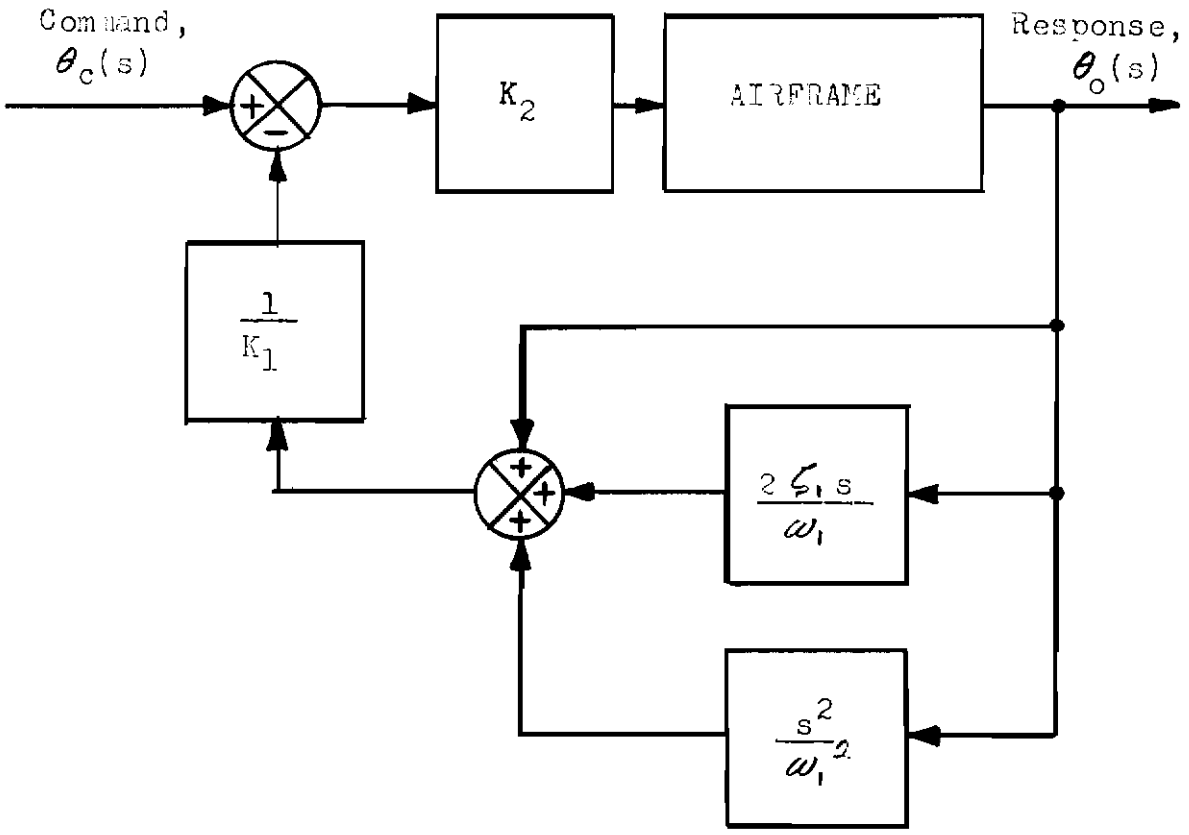

Fig. 2b SHORT PERIOD CONTROL CONFIGURATION

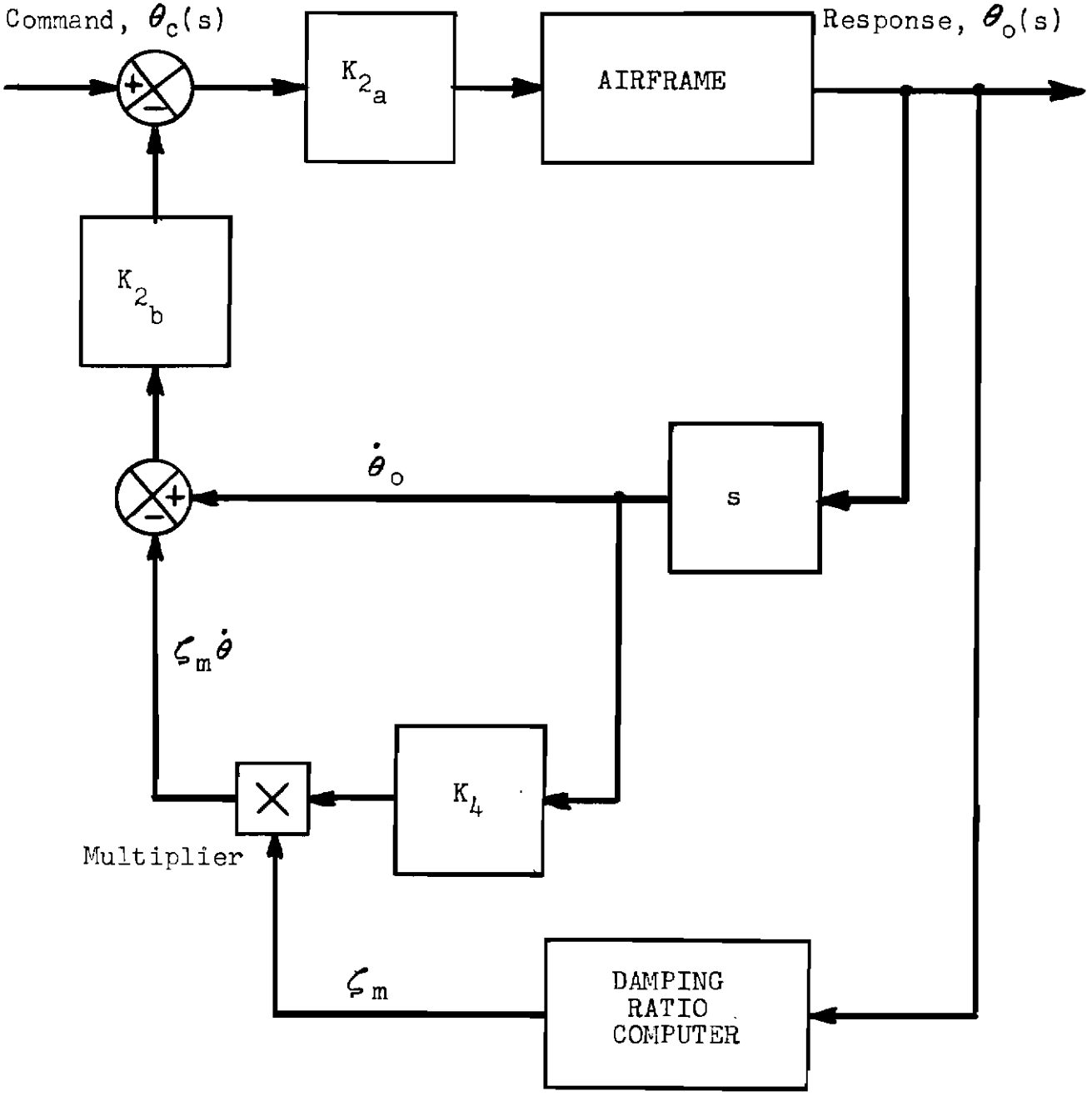

Fig. 3a DAMPING RATIO FEEDBACK CONCEPT

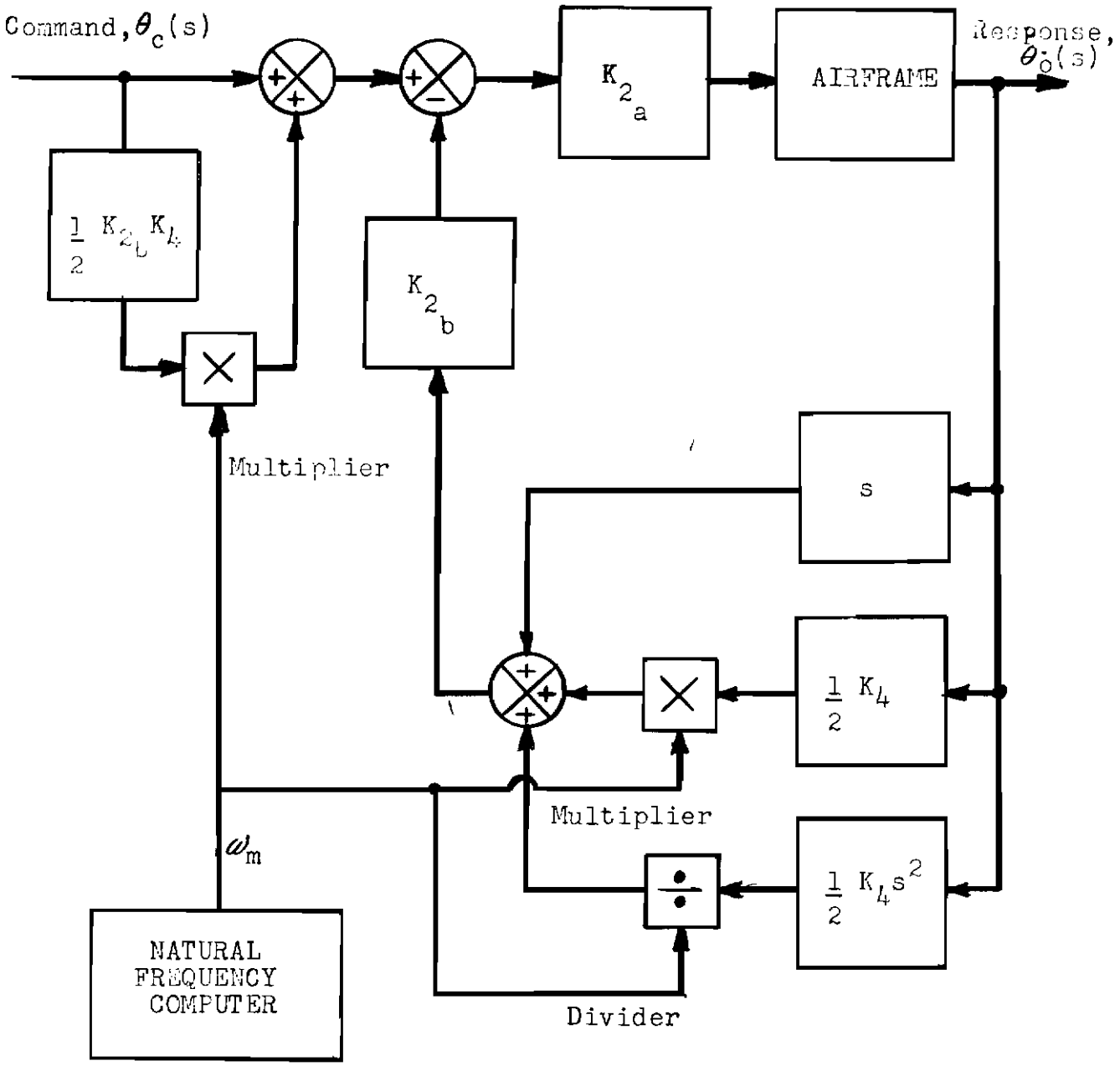

Fig. 3b DAMPING RATIO FEEDBACK CONCEPT

that of negative feedback, it is seen that the proper compensation is achieved.

The over-all amount of rate feedback is determined by the over-all loop gain. Two adjustments of loop gain are provided by K_{2_a} and K_{2_b}. One is in the forward loop and one is in the feedback loop. This arrangement allows the closed loop steady state gain to be adjusted independently. Steady state gain, defined as the steady state value of the ratio $\frac{|\theta_0|}{|\theta_C|}$, is the equal to the forward loop gain divided by the product of the forward and feedback loop gains plus one. Therefore, the steady state gain is adjustable by fixing the value of K_{2_a} in relation to the value of the product of K_{2_a} and K_{2_b}. The over-all amount of rate feedback on the other hand is adjustable by fixing the product of K_{2_a} and K_{2_b} only.

Zero output damping reduces the gain of the auxiliary rate feedback loop, K_4, to zero (Fig. 3a). Therefore, at flight conditions where the airframe is neutrally stable (zero output damping) the gain K_2 (the product of K_{2_a} and K_{2_b}) alone determines the stability augmentation. This observation provides a convenient method of determining the proper adjustment of K_2. On the other hand, when the airframe response is damped, then the gain K_4 determines the amount of negative feedback cancellation. At flight conditions when the free airframe is satisfactorily damped, positive and negative feedback should cancel one another since no compensation is necessary. This condition provides a method of adjusting K_4. Should the airframe become unstable, the computed damping ratio signal must change sign in order to increase the over-all negative feedback.

Damping ratio is a second order characteristic; its computation must thus be based on the assumption that the pitch response resembles a second order response in the short period mode. Experience has shown that this assumption is justified. A second order relationship may be represented in general by an equation of the form

$$\frac{1}{\omega_0^2}\ddot{\theta}_0 + \frac{2\zeta_0}{\omega_0}\dot{\theta}_0 + \theta_0 = \theta_C \qquad (6)$$

By rearranging terms, Equation 6 may be written

$$\zeta_0 \dot{\theta}_0 = -\frac{\omega_0}{2} \theta_C - \frac{\omega_0}{2} \theta_0 - \frac{1}{2\omega_0} \ddot{\theta}_0 . \quad (7)$$

From Equation 7 it is deduced that positive pitch rate feedback multiplied by measured damping ratio, ζ_m, (Fig. 3a) may be replaced by negative feedback of pitch attitude and pitch acceleration plus additive input command compensation and appropriately measured natural frequency correction, ω_m. This substitution is illustrated in Figure 3b.

The mechanization of the relation expressed by Equation 7 as shown in Figure 3b, would be complex since the quantity ω_m must be injected as a multiplying factor in two of the loops and as a dividing factor in a third loop. The exact short period natural frequency of the airframe, ω_0, is itself not readily measurable nor computable from the output response. In the system discussed herein, this difficulty was avoided by ignoring variation in ω_0 and by setting ω_m, in Figure 3b, equal to a predetermined constant C. This simplification allows a linear analysis of the system since all three feedback loops have constant gains. As another result of this assumption, the additive compensation becomes a fixed gain compensation and may be included into the gain terms inside the control loop. Thus a quasi damping ratio ζ' may be defined by the following equation in terms of the airframe response in pitch.

$$\zeta' \dot{\theta}_0 = -\frac{C}{2} \theta_0 - \frac{1}{2C} \ddot{\theta}_0 . \quad (8)$$

Incorporation of this relationship into the block diagram leads to the system illustrated in Figure 4.

There is no essential difference between the systems shown in Figures 2b and 4. An analysis of the character of the performance of the control represented by these systems would be identical in basic treatment and the results would be the same.

The investigation discussed in this report was performed as part of a study and evaluation of the nonlinear damping ratio feedback system illustrated in Figure 3a. The particular simplifying assumptions which were made in the linearization of the control system in order to facilitate its mathematical analysis has led to the system shown in Figure 4. Because another simpler and well-known method of control synthesis led to the same configuration (Fig. 2b), it was

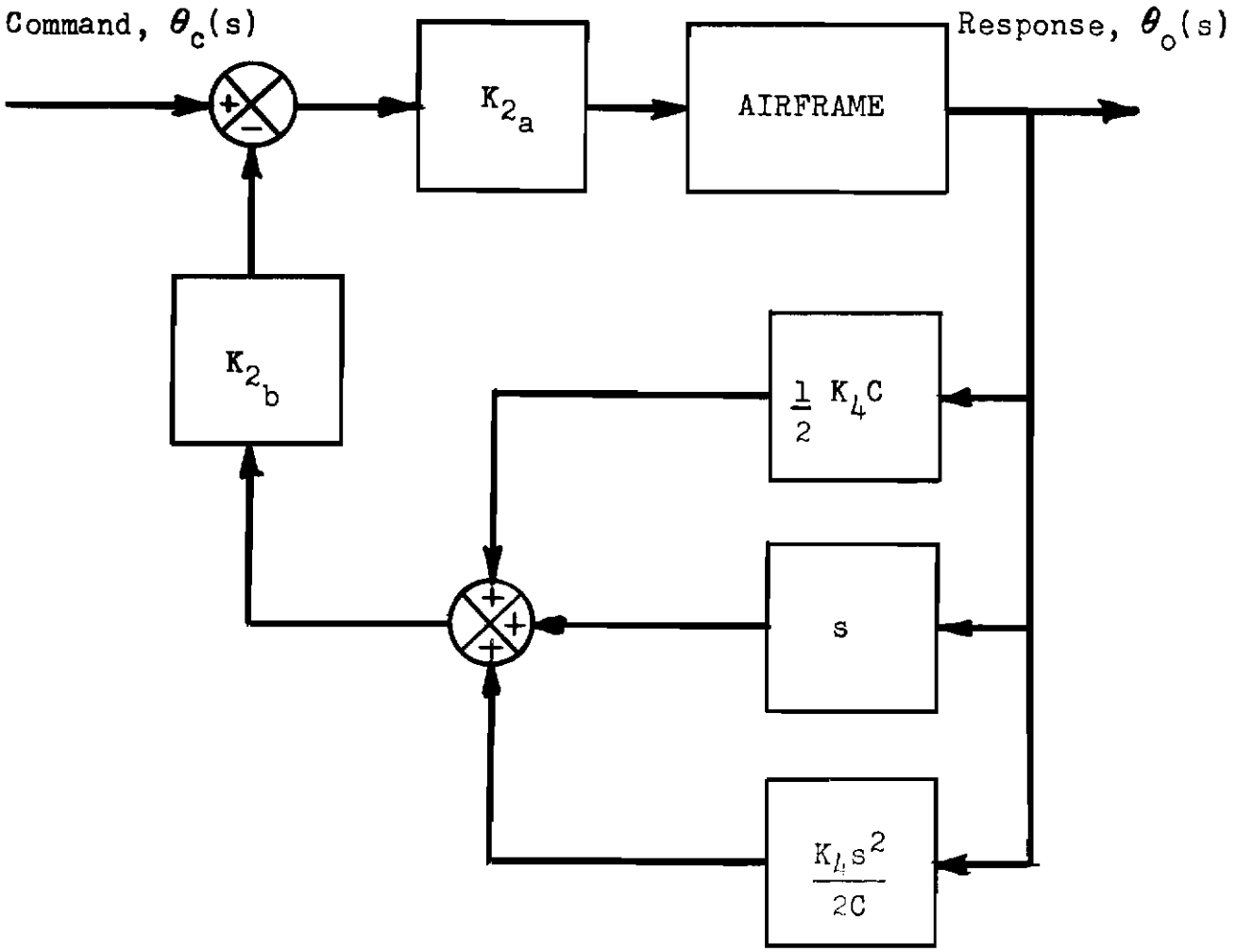

Fig. 4 SIMPLIFIED DAMPING RATIO FEEDBACK CONTROL

proper to introduce both approaches independently. However, the analysis of the final control form (Fig. 2b or 4) will be presented independently of the original approach.

Further details on each of the approaches mentioned and other aspects which emphasize the difference between them may be found in Reference 1.

ANALYSIS OF SELF-ADAPTIVE METHOD IN TYPICAL IDEALIZED FLIGHT CONTROL SYSTEM

The method of self-adaptive control discussed earlier may be incorporated within several control channels of an aircraft stability augmentation system. The feedback quantities may differ in each channel; the amount of stability correction needed may vary; but the basic operations of the control system will remain the same. In general, the longitudinal short period mode motion is the most critical in stability control. For this reason the method will be analyzed as it would be applied in a typical short period mode control. The short period motion will be assumed to be independent of other airframe modes; hence it is sufficient to represent the airframe by its short period dynamics.

In this portion of the analysis the control system will be assumed to have ideal dynamic characteristics (i.e., the dynamics of the instrumentation and of the hydraulic servo are neglected).

Typical of airframe short period dynamics are the second order characteristics represented by Equation 5. The complete airframe-control system configuration to be analyzed is illustrated in Figure 5.

By employing the formula given in Equation 1, the transfer function of the over-all control loop illustrated in Figure 5 is obtained as follows:

$$\frac{\theta_0(s)}{\theta_C(s)} = \frac{\dfrac{K_0K_2}{1 + \dfrac{K_0K_2}{K_1}}}{\dfrac{1}{\omega_0^2}\left[\dfrac{1 + \dfrac{\omega_0^2K_0K_2}{\omega_1^2K_1}}{1 + \dfrac{K_0K_2}{K_1}}\right]s^2 + \left[\dfrac{\dfrac{2\zeta_0}{\omega_0} + \dfrac{2\zeta_1K_0K_2}{\omega_1K_1}}{1 + \dfrac{K_0K_2}{K_1}}\right]s + 1} \qquad (9)$$

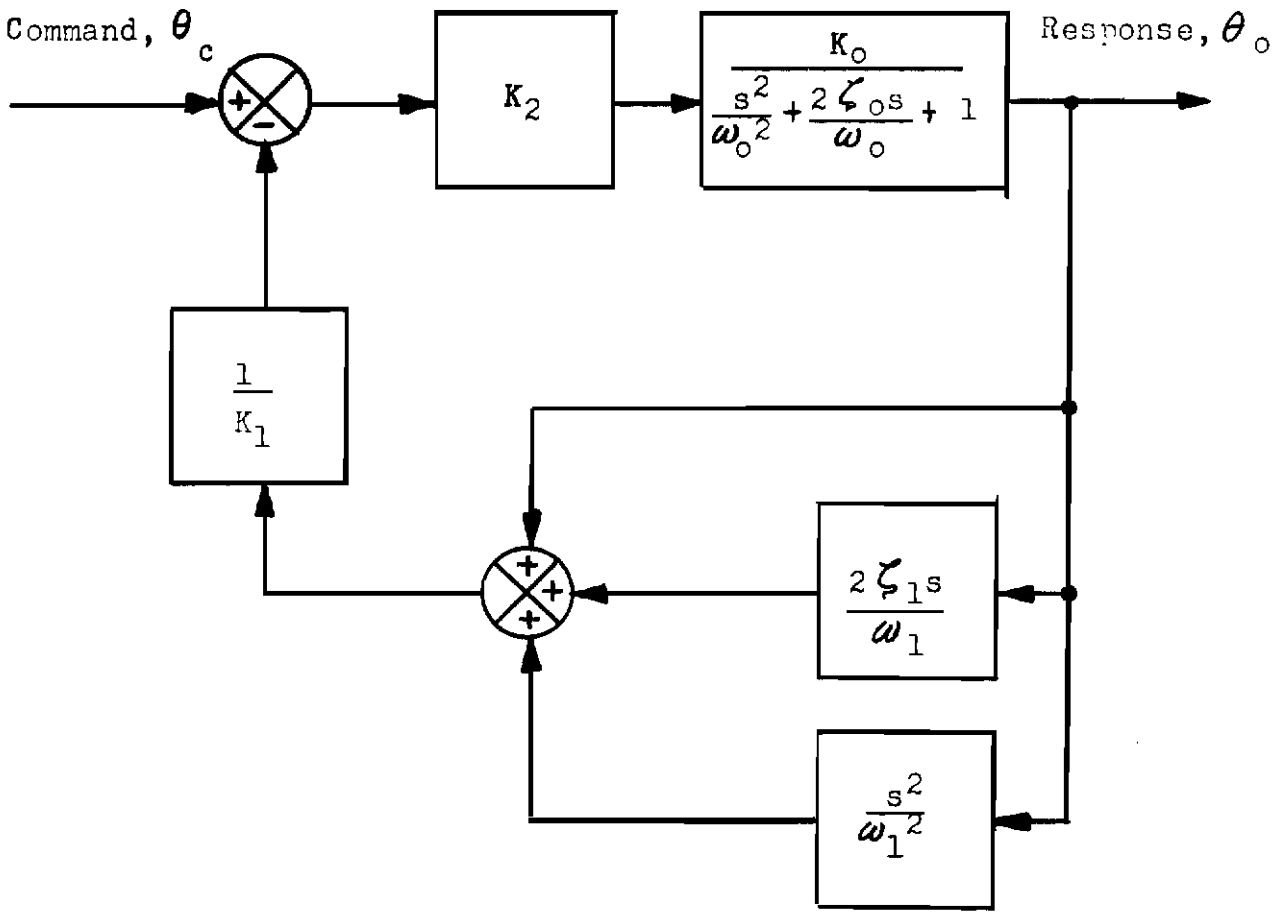

Fig. 5 DIAGRAM OF CONTROL APPLICATION WITHOUT INSTRUMENTATION

Equation 9 is of the general form

$$\frac{\theta_0(s)}{\theta_C(s)} = \frac{K_3}{\frac{s^2}{\omega_3^2} + \frac{2\zeta_3 s}{\omega_3} + 1}, \tag{10}$$

where

$$K_3 = \frac{K_o K_2}{1 + \frac{K_o K_2}{K_1}}, \tag{11}$$

$$\omega_3 = \omega_o \sqrt{\frac{1 + \frac{K_o K_2}{K_1}}{1 + \frac{\omega_0^2 K_o K_2}{\omega_1^2 K_1}}}, \tag{12}$$

and

$$\zeta_3 = \frac{\zeta_0 + \frac{\omega_0 \zeta_1 K_o K_2}{\omega_1 K_1}}{\sqrt{1 + \frac{K_o K_2}{K_1}} \sqrt{1 + \frac{\omega_0^2 K_o K_2}{\omega_1^2 K_1}}} \tag{13}$$

The quantity K_2 represents the adjustable gain in the control loop. It can be seen that Equations 11, 12, and 13 can be reduced, respectively, to

$$K_3 \approx K_1, \tag{14}$$

$$\omega_3 \approx \omega_1, \tag{15}$$

and

$$\zeta_3 \approx \zeta_1 \tag{16}$$

when K_2 is sufficiently large to satisfy the following inequalities

$$\frac{K_o K_2}{K_1} \gg 1, \tag{17}$$

$$\frac{\omega_0^2 K_o K_2}{\omega_1^2 K_1} \gg 1, \tag{18}$$

and

$$\frac{\omega_0 \zeta_1 K_o K_2}{\omega_1 \zeta_0 K_1} \gg 1 \ . \tag{19}$$

When K_2 is not sufficiently large to satisfy the above inequalities, the parameters K_3, ω_3, and ζ_3 lie between their ideal values, K_1, ω_1, and ζ_1 and their respective free airplane values K_o, ζ_0, and ζ_0. The degree of compensation achieved is shown graphically in Figures 6 and 7 as a function of the value of $\frac{K_o K_2}{K_1}$. These graphs represent the behavior of the system illustrated in Figure 5. The curves shown were obtained by calculating the roots of the equation

$$\frac{1}{\omega_0^2}\left[\frac{1+\frac{\omega_0^2 K_o K_2}{\omega_1^2 K_1}}{1+\frac{K_o K_2}{K_1}}\right]s^2+\left[\frac{\frac{2\zeta_0}{\omega_0}+\frac{2\zeta_1 K_o K_2}{\omega_1 K_1}}{1+\frac{K_o K_2}{K_1}}\right]s+1=0 \qquad (20)$$

for all combinations of the following values

ω_0 = 1, 2, 4, 6 and 10

ζ_0 = 0, 0.2, 0.707 and 1.0

$\frac{K_o K_2}{K_1}$ = 0.5, 1.0, 2, 4, 10, 20 , 40 and 100

ω_1 = 2

ζ_1 = 0.707.

Each of the dashed curves in Figure 6 shows the locus of the roots of Equation 20 as the loop gain $\frac{K_o K_2}{K_1}$ varies from zero to infinity. Each curve represents an airframe at a particular flight condition. As $\frac{K_o K_2}{K_1}$ increases, all the curves approach the design point (ω_1, ζ_1). The solid lines in this figure describe the boundaries of the short period response of the closed-loop system for an airframe whose open-loop response lies within the region bounded by

$$1 \text{ radian per second} \leq \omega_0 \leq 10 \text{ radians per second}$$

$$0 \leq \zeta_0 \leq 1.0$$

As the loop gain is increased, the boundary encloses a smaller and smaller area about the design point.

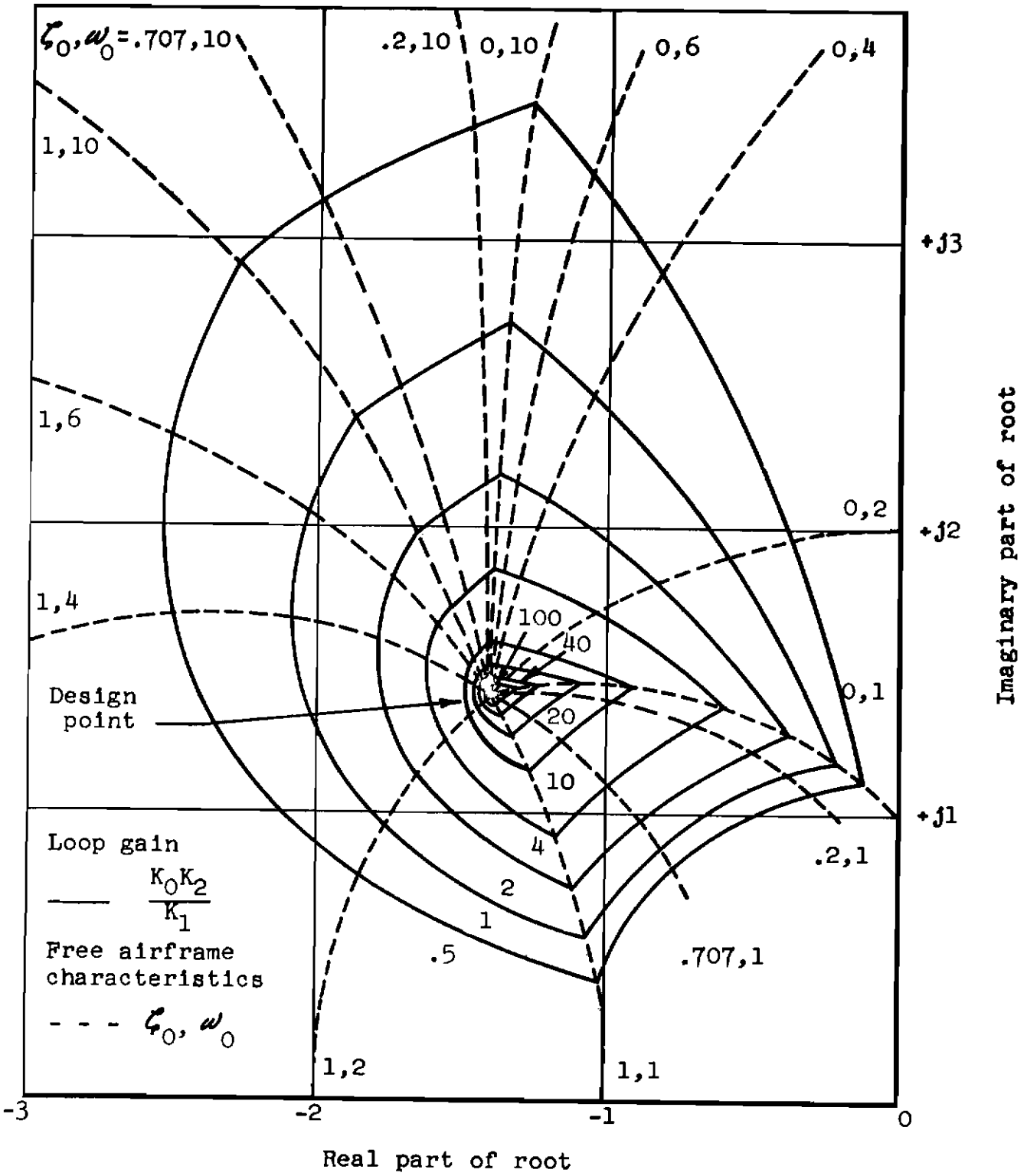

Fig. 6a LOCUS OF ROOTS OF CHARACTERISTIC EQUATION OF CLOSED-LOOP SYSTEM FOR DIFFERENT LOOP GAINS AND FREE AIRFRAME CHARACTERISTICS

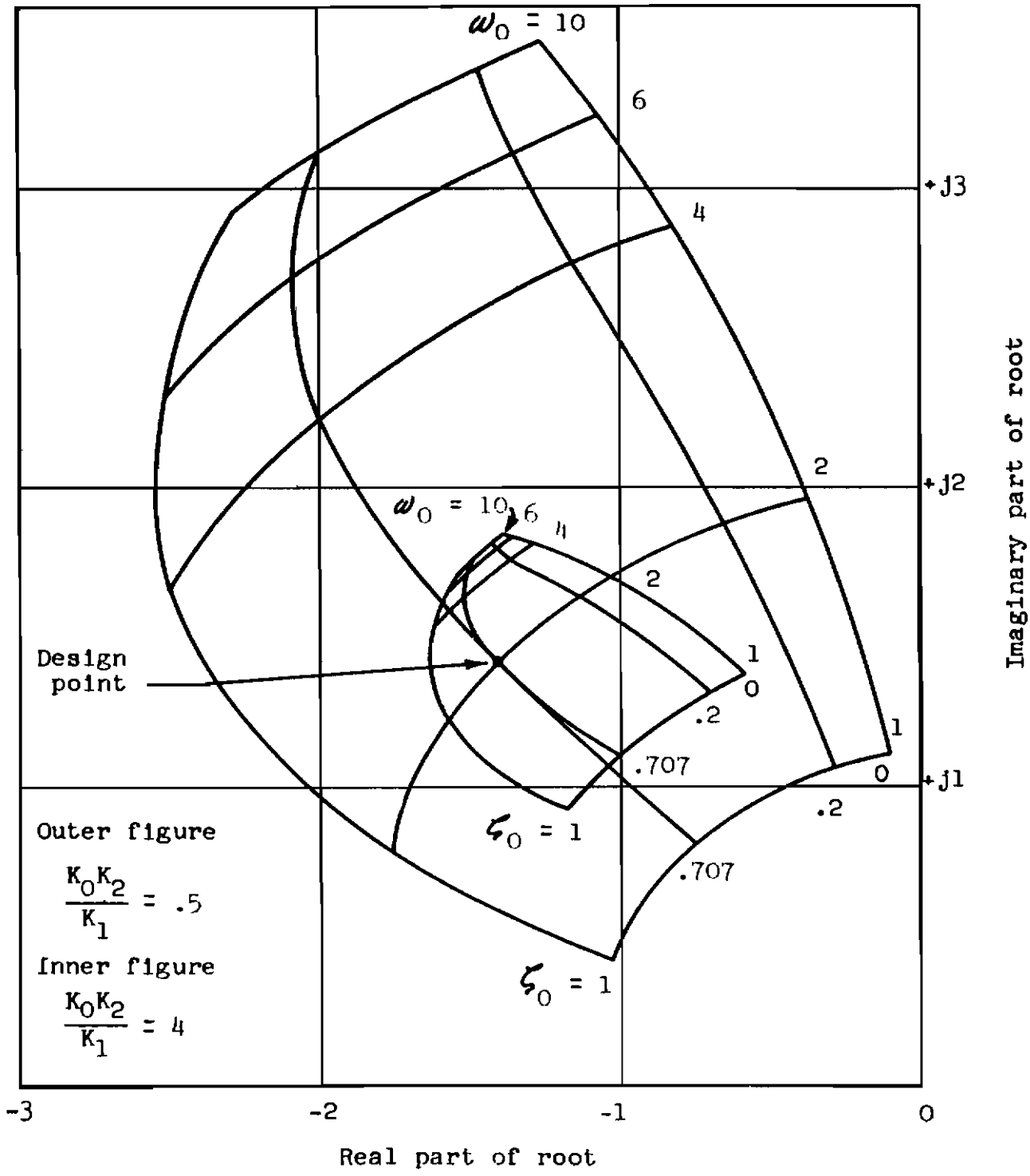

Fig. 6b LOCUS OF ROOTS OF CHARACTERISTIC EQUATION OF CLOSED-LOOP SYSTEM FOR DIFFERENT LOOP GAINS AND FREE AIRFRAME CHARACTERISTICS

In Figure 7 two particular values of loop gain have been selected to illustrate the location of the roots of the closed loop for all possible combinations of ω_0 and ζ_0 listed on the preceding page. The curves which are somewhat radial from the origin are loci of constant ζ_0; those which are approximately circular about the origin represent loci of constant ω_0.

The preceding discussion of the self-adaptive control method indicates that ideal performance characteristics are attainable simply by providing a sufficiently large control loop gain. From Equation 10 it can be seen that the closed-loop system used for illustration is of the second order. Since free airframe damping was assumed to be greater than or equal to zero and negative feedback was chosen, it follows that the system shown in Figure 5 cannot become unstable at any loop gain.

Actual aircraft-flight control system combinations possess physical characteristics which must be described by differential equations of higher orders than second. In such an instance Equations 11, 12, and 13 are no longer exactly correct so that inequalities given in Equations 17, 18, and 19 are not sufficient to produce the approximations given in Equations 14, 15, and 16. This problem is investigated in the next section.

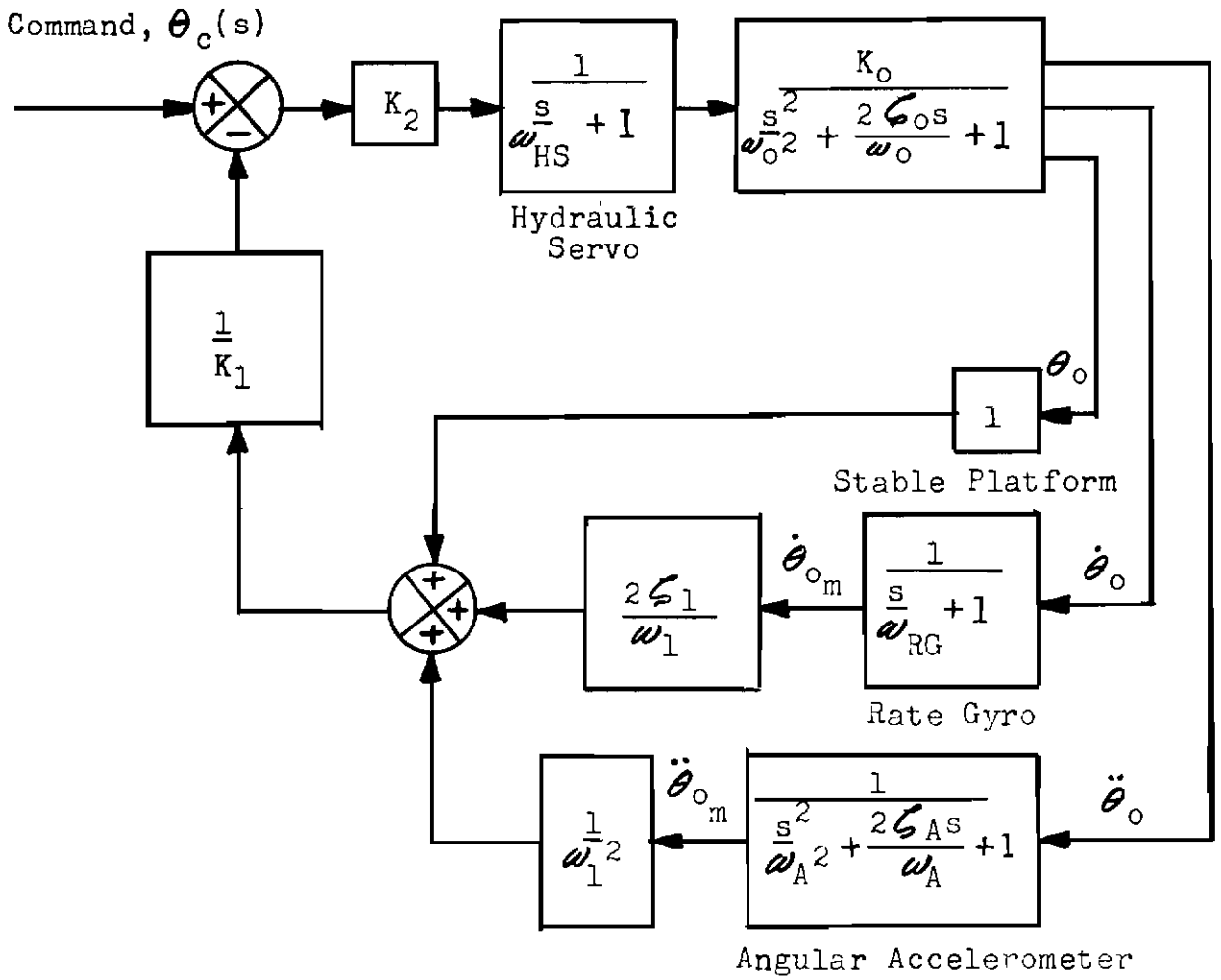

Fig. 7 DIAGRAM OF CONTROL APPLICATION INCLUDING INSTRUMENTATION

ANALYSIS AND SYNTHESIS OF TYPICAL FLIGHT CONTROL SYSTEM WITH SENSING INSTRUMENTS AND HYDRAULIC SERVO

Description of Additional Components

Components which contribute chiefly to higher order characteristics in aircraft control systems are those which convert electrical command signals into motion of the airframe control surfaces and those which measure the airframe motion and transduce this motion into electrical signals. In order to illustrate the effects of these components on the self-adaptive system described previously, the following will be required: a stable platform to measure the pitch angle of the airframe, a rate gyro to measure pitch angular velocity, an angular accelerometer to measure pitch angular acceleration, and a hydraulic servo to convert command signals into elevator deflections.

In the block diagram in Figure 7 the location of each of these components in the loop and the form of their transfer functions are shown. Only the major dynamic effects were included. The performance of the self-adaptive control was then calculated for the expected ranges of values of these dynamic effects. The inclusion of these components into the system introduces additional phase lag which may produce system instability at sufficiently large loop gains. The ranges which were selected were considered to be sufficient to show the trends in system stability and accuracy.

The Hydraulic Servo Actuator

Flow type hydraulic actuators produce actuator piston rates of displacements that are essentially proportional to their respective control valve positions. Transient dynamics appear as a result of actuator piston inertia, fluid compressibility, fluid leakage, line lags, and valve inertia. Some of these factors are often neglected; however, when actuator and valve position are linked by mechanical feedback, the complete diagram of a typical hydraulic servo system may be represented as in Figure 8 below.

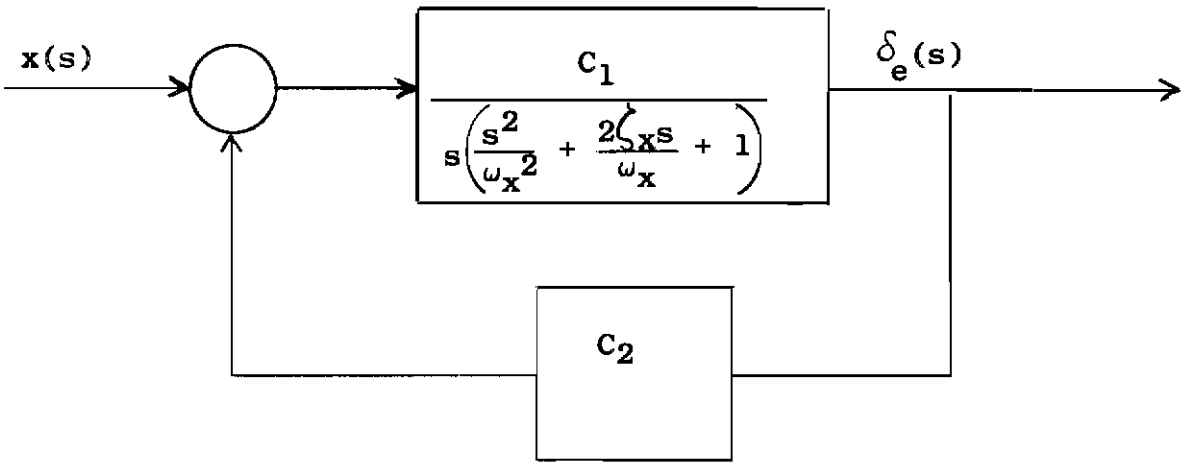

Fig. 8 - DIAGRAM OF TYPICAL HYDRAULIC SERVO SYSTEM

The second order lag factor characterized by the term ω_x and ζ_x represent the inertia and compressibility effects mentioned previously. For representative hydraulic systems, typical values of ω_x are in the neighborhood of 600 radians per second and typical values of ζ_x are near zero. In the discussions which follow, these dynamics will be neglected since their frequency characteristics are outside the frequency range of the airplane. The closed-loop transfer function of the hydraulic system illustrated in Figure 9 is then reduced to the function

$$\frac{\delta_e(s)}{x(s)} = \frac{\frac{1}{C_2}}{\frac{s}{C_1 C_2} + 1} .$$

The hydraulic servo characteristic frequency ω_{HS}, represented in Figure 8, is adjustable by changing the servo loop gain C_1C_2. The following values were selected in this analysis

$$20 \text{ radins per second} \leq \omega_{HS} \leq 50 \text{ radins per second.}$$

The gain of the hydraulic servo was assumed to be unity.

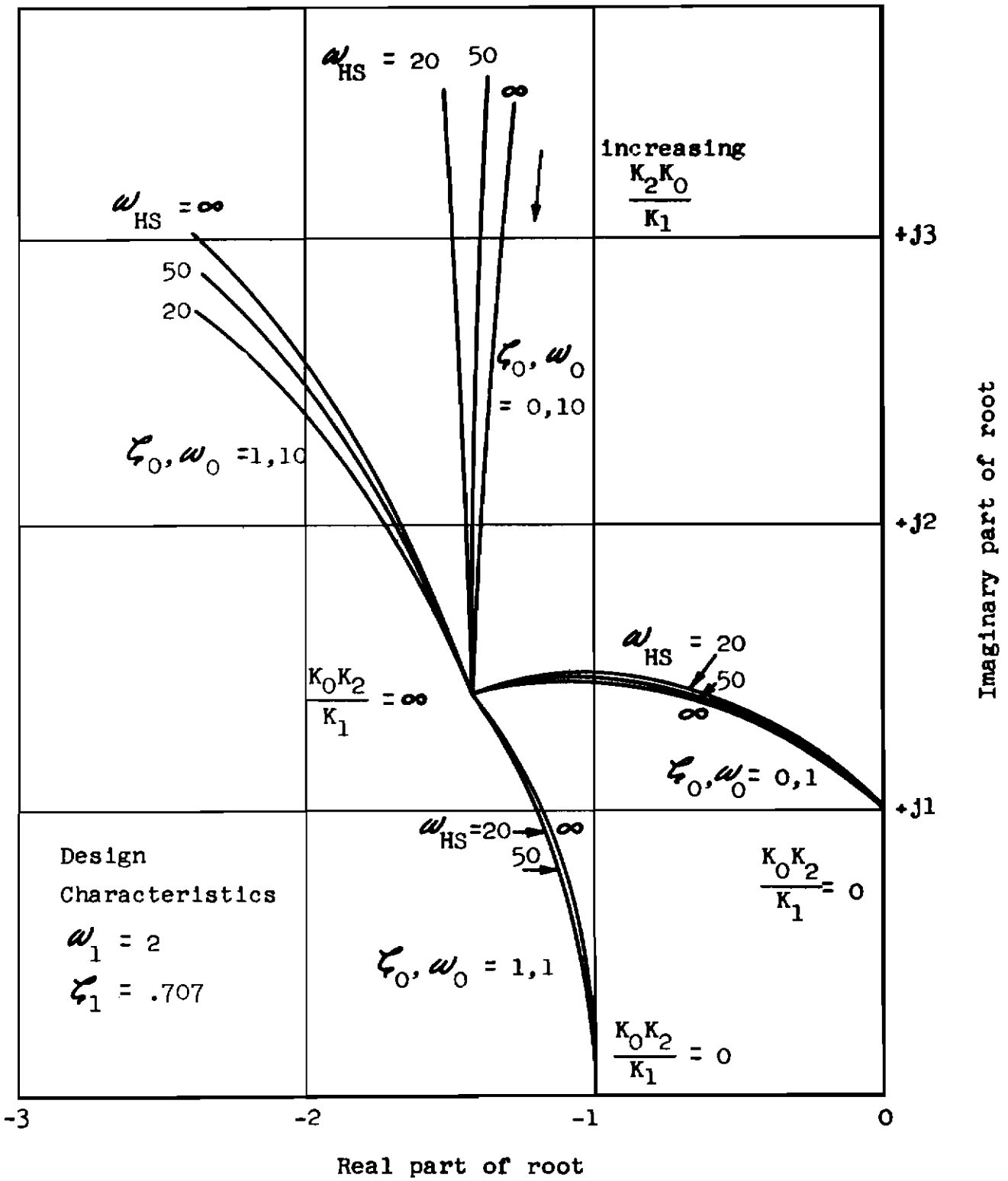

Fig. 9 EFFECT OF HYDRAULIC SERVO ON CLOSED-LOOP, SHORT PERIOD CHARACTERISTICS FOR DIFFERENT LOOP GAINS AND FREE AIRFRAME CHARACTERISTICS

The Rate Gyro

A rate gyro is a single-degree-of-freedom gyro with an elastic restraint on its movement about the free axis so that the angular deflection of this axis is proportional to the angular velocity about the input axis fixed to the airplane. Factors which have an effect on the dynamic response of a rate gyro are essentially the compliance of the elastic restraint, the moment of inertia about the free axis, and the viscous damping introduced to damp the free gimbal deflection.

In most practical cases the transient behavior of rate gyros may be represented mathematically by a second order system. The corresponding transfer function may be written in the form

$$\frac{\dot{\theta}_{0_m}(s)}{\dot{\theta}_0(s)} = \frac{\frac{H}{K_r}}{\left(\frac{H^2}{K_i K_r} + \frac{J_r}{K_r}\right) s^2 + \frac{f_r}{K_r} s + 1} .$$

Typical rate gyros have natural frequencies ranging approximately from 40 to 500 radians per second. The usually desired value of damping ratio ranges from 0.6 to 0.8. Damping ratio is known to vary with ambient temperature. A temperature change spanning 250°F, for example, will vary damping ratio from approximately 0.3 to 2.0 in a typical case. Furthermore, an increase in viscosity is known to increase the gyro moment of inertia. This increase in moment results in a decrease in natural frequency. With a damping ratio less than unity, the rate gyro characteristics are represented by a second order transfer function with two complex poles. With a damping ratio greater than unity, two real poles are present which from two first order terms, one of which will have a dominant effect on phase lag.

For these reasons two representations of the rate gyro characteristics were considered:

$$\frac{\dot{\theta}_{0_m}(s)}{\dot{\theta}_0(s)} = \frac{C_3}{\frac{s^2}{\omega_{RG}} + \frac{2\zeta_{RG}s}{\omega_{RG}} + 1}$$

and $$\frac{\dot{\theta}_{0_m}(s)}{\dot{\theta}_0(s)} = \frac{C_3}{\left(\frac{s}{\omega_{RG_1}} + 1\right)\left(\frac{s}{\omega_{RG_2}} + 1\right)}$$

These representations were compared by considering two typical cases, one involving a damping ratio of 0.7 and an undamped natural frequency of 100 radians per second and the other a damping ratio of 1.45 and the first order term characteristics ω_{RG_1} = 40 radians per second and ω_{RG_2} is sufficiently large to be negligible in its effect on the system as compared to ω_{RG_1}. It is shown in a later section that there is no significant change in the effects of rate gyro dynamics on system stability whether one or the other of the above representations is used. For the above reasons, the simplest of the two representation appears justifiable; hence in this analysis the rate gyro characteristics were represented by

$$\frac{\dot{\theta}_{0_m}(s)}{\dot{\theta}_0(s)} = \frac{C_3}{\frac{s}{\omega_{RG}} + 1} .$$

The following values of ω_{RG} were assumed in this analysis.

$$40 \text{ radians per second} \leq \omega_{RG} \leq 60 \text{ radians per second}$$

The gain of the rate gyro was assumed to be unity.

The Stable Platform

Three-axis, stabilized platform, normally used in aircraft, comprise three gyros for the three orthogonal axes and a gimbal system driven by servomotors controlled by the gyro outputs. The platform is usually large enough to mount instruments or devices which are required to be in a stabilized position. The angular position of the various gimbals referred to the platform is an indication of the attitude of the airframe about the various axes of inertial space.

The servomotors which stabilize the platform usually have a sufficiently rapid response so that their dynamics do not affect the outputs within the frequency range of interest. The dynamics of the platform suspension system may likewise be neglected for practical purposes. For these reasons the stable platform will be considered to be a perfect transducer.

The Angular Accelerometer

Typical angular accelerometers include a dynamically balanced mass suspended so that it has only one degree of freedom. The mass rotates against a restraining spring and damper; this movement is sensed by a transducer. The angular acceleration of the instrument case is proportional to the angular displacement of the mass with respect to the case. The transfer function of the instrument may be shown to be of the form

$$\frac{\ddot{\theta}_{0_m}(s)}{\dot{\theta}_0(s)} = \frac{\frac{I}{k}}{\frac{I}{k}s^2 + \frac{f}{k}s + 1} .$$

Typical accelerometers have natural frequencies ranging from 50 to 600 radians per second. The usually desired value of damping ratio is 0.6 since this value gives a good steady state sinusoidal response and a reasonable overshoot for transient inputs. In this analysis the following ranges of natural frequency, ω_A, and damping ratio ζ_A were chosen

$$50 \text{ radians per second} \leq \omega_A \leq 250 \text{ radians per second}$$

$$0.25 \leq \zeta_A \leq 2.0$$

The gain of the accelerometer was assumed to be unity.

Effects of Added Components on Short-Period Characteristics at Various Loop Gains

The effect of added components on the short period correction may be found by calculating the closed-loop transfer function of the over-all system depicted in Figure 7. By using the formula given in Equation 1, the following result is easily obtained.

$$\frac{\theta_0(s)}{\theta_C(s)} = \frac{\dfrac{K_o K_2}{\left(\dfrac{s}{\omega_{HS}} + 1\right)\left(\dfrac{s^2}{\omega_0^2} + \dfrac{2\zeta_0 s}{\omega_0} + 1\right)}}{1 + \dfrac{K_o K_2 \left[\dfrac{s^2}{\omega_1^2\left(\dfrac{s^2}{\omega_A^2} + \dfrac{2\zeta_A s}{\omega_A} + 1\right)} + \dfrac{2\zeta_1 s}{\omega_1\left(\dfrac{s}{\omega_{RG}} + 1\right)} + 1\right]}{K_1\left(\dfrac{s}{\omega_{HS}} + 1\right)\left(\dfrac{s^2}{\omega_0^2} + \dfrac{2\zeta_0 s}{\omega_0} + 1\right)}} \cdot \quad (23)$$

When K_2 is made sufficiently large so that

$$\frac{\left[\dfrac{s^2}{\omega_1^2\left(\dfrac{s^2}{\omega_A^2} + \dfrac{2\zeta_A s}{\omega_A} + 1\right)} + \dfrac{2\zeta_1 s}{\omega_1\left(\dfrac{s}{\omega_{RG}} + 1\right)} + 1\right] K_o K_2}{K_1\left(\dfrac{s}{\omega_{HS}} + 1\right)\left(\dfrac{s^2}{\omega_0^2} + \dfrac{2\zeta_0 s}{\omega_0} + 1\right)} \gg 1, \quad (24)$$

then Equation 23 is reduced to

$$\frac{\theta_0(s)}{\theta_C(s)} = \frac{K_1}{\dfrac{s^2}{\omega_1^2\left(\dfrac{s^2}{\omega_A^2} + \dfrac{2\zeta_A s}{\omega_A} + 1\right)} + \dfrac{2\zeta_1 s}{\omega_1\left(\dfrac{s}{\omega_{RG}} + 1\right)} + 1} \cdot \quad (25)$$

Two important results may be seen immediately. The dynamics of the hydraulic servo or of the airframe do not appear in Equation 25. In fact any element in the forward path of the control system (Fig. 7) has no effect on the over-all dynamics of the system at high loop gains (it is assumed that

these elements are linear). Also, no matter now large the gain K_2 is chosen, the system will not approach the ideal characteristics defined by the transfer function

$$\frac{\theta_0(s)}{\theta_C(s)} = \frac{K_1}{\frac{s^2}{\omega_1^2} + \frac{2\zeta_1 s}{\omega_1} + 1} \cdot \tag{26}$$

The reason for this is the dynamic effect of the accelerometer and the rate gyro. These effects may be evaluated in Equation 23 by inserting different values of the terms ω_{HS}, ω_{RG}, ω_A and ζ_A.

It is convenient to first rewrite Equation 23 as follows:

$$\frac{\theta_0(s)}{\theta_C(s)} = \frac{K_0K_2}{\left(\frac{s}{\omega_{HS}}+1\right)\left(\frac{s^2}{\omega_0^2}+\frac{2\zeta_0 s}{\omega_0}+1\right) + \frac{K_0K_2}{K_1}\left[\frac{s^2}{\omega_1^2\left(\frac{s^2}{\omega_A^2}+\frac{2\zeta_A s}{\omega_A}+1\right)} + \frac{2\zeta_1 s}{\omega_1\left(\frac{s}{\omega_{RG}}+1\right)} + 1\right]} \tag{27}$$

The dynamic characteristics may now be obtained by computing the roots of the equation formed by setting the denominator of Equation 27 equal to zero as follows:

$$\left(\frac{s}{\omega_{HS}}+1\right)\left(\frac{s^2}{\omega_0^2}+\frac{2\zeta_0 s}{\omega_0}+1\right) + \frac{K_0K_2}{K_1}\left[\frac{s^2}{\omega_1^2\left(\frac{s^2}{\omega_A^2}+\frac{2\zeta_A s}{\omega_A}+1\right)} + \frac{2\zeta_1 s}{\omega_1\left(\frac{s}{\omega_{RG}}+1\right)} + 1\right] = 0. \tag{28}$$

Figures 9, 10 and 11 show the loci of the short period roots of Equation 28 for different values of ω_{HS}, ω_{RG}, ω_A and ζ_A as the gain parameter $\frac{K_oK_2}{K_1}$ is varied from zero to infinity.

Four combinations of free airframe characteristics were chosen to encompass the widest possible range of flight conditions; these are as follows:

ω_0	ζ_0
1	0
1	1
10	0
10	1

The ideal characteristics were chosen as follows:

$$\omega_1 = 2 \text{ radians per second}$$
$$\zeta_1 = 0.707.$$

The separate effects of the hydraulic servo, the rate gyro, and the accelerometer are discussed below.

Effect of the Hydraulic Servo

The effects of the hydraulic servo alone (Fig. 9) were obtained by neglecting the rate gyro and accelerometer dynamics in Equation 27.

$$\frac{\theta_0(s)}{\theta_C(s)} = \frac{K_oK_2}{\left(\frac{s}{\omega_{HS}}+1\right)\left(\frac{s^2}{\omega_0^2}+\frac{2\zeta_0 s}{\omega_0}+1\right)+\frac{K_oK_2}{K_1}\left(\frac{s^2}{\omega_1^2}+\frac{2\zeta_1 s}{\omega_1^2}+1\right)}. \quad (29)$$

As $\frac{K_oK_2}{K_1}$ approaches zero, the feedback path becomes open circuited, and Equation 29 approaches

$$\frac{\theta_0(s)}{\theta_C(s)} = \frac{K_oK_2}{\left(\frac{s}{\omega_{HS}}+1\right)\left(\frac{s^2}{\omega_0^2}+\frac{2\zeta_0 s}{\omega_0}+1\right)}. \quad (30)$$

As $\frac{K_o K_2}{K_1}$ approaches infinity, Equation 29 approaches

$$\frac{\theta_0(s)}{\theta_C(s)} = \frac{K_1}{\frac{s^2}{\omega_1^2} + \frac{2\zeta_1 s}{\omega_1} + 1} \quad . \tag{31}$$

These results indicate that with no feedback the short period characteristics are defined by the roots of the equation

$$\frac{s^2}{\omega_0^2} + \frac{2\zeta_0 s}{\omega_0} + 1 = 0, \tag{32}$$

and with a large feedback loop gain the characteristics are defined by the roots of the equation

$$\frac{s^2}{\omega_1^2} + \frac{2\zeta_1 s}{\omega_1} + 1 = 0 \quad . \tag{33}$$

Therefore, at both extremes of loop gain, the short period response is independent of the hydraulic servodynamics.

In the midrange values of loop gain, the system dynamics are defined by the roots of the equation

$$\left(\frac{s}{\omega_{HS}} + 1\right)\left(\frac{s^2}{\omega_0^2} + \frac{2\zeta_0 s}{\omega_0} + 1\right) + \frac{K_o K_2}{K_1}\left(\frac{s^2}{\omega_1^2} + \frac{2\zeta_1 s}{\omega_1} + 1\right) = 0. \tag{34}$$

In Figure 9 the effect of loop gain is shown for two finite values of hydraulic servo characteristic frequency, namely, 20 and 50 radians per second and an infinite frequency. The curves for which the frequency is infinite represent the system in which an ideal hydraulic servo is used, that is, one

with a unity transfer function. As the characteristic frequency, ω_{HS}, is decreased, it can be seen from Figure 9 that the short period roots deviate further and further from the ideal case.

From previous analysis it has been shown that at both extremes of loop gain the servodynamics do not affect the short period response. The maximum deviation resulting from the servodynamics occurs between these two loop gain extremes. This midrange effect of the hydraulic servo appears to be more pronounced for those conditions in which the free airframe short period natural frequency, ω_0, is the largest. As would be expected, this result indicates that the closer together are the values of ω_0 and ω_{HS}, the greater will be the interactive effect between the servodynamics and the short period dynamics.

Effect of the Rate Gyro

The effects of the rate gyro alone (Fig. 10) are calculated from Equation 27 by neglecting the hydraulic servodynamics and the accelerometer dynamics. This equation may then be written in the following form:

$$\frac{\theta_0(s)}{\theta_C(s)} = \frac{K_oK_2}{\left(\frac{s^2}{\omega_0^2} + \frac{2\zeta_0 s}{\omega_0} + 1\right) + \frac{K_oK_2}{K_1}\left(\frac{s^2}{\omega_1^2} + \frac{2\zeta_1 s}{\omega_1\left(\frac{s}{\omega_{RG}} + 1\right)} + 1\right)} . \tag{35}$$

As $\frac{K_oK_2}{K_1}$ approaches zero, Equation 35 approaches

$$\frac{\theta_0(s)}{\theta_C(s)} = \frac{K_oK_2}{\frac{s^2}{\omega_0^2} + \frac{2\zeta_0 s}{\omega_0} + 1} , \tag{36}$$

and as $\frac{K_o K_2}{K_1}$ approaches infinity, Equation 35 approaches

$$\frac{\theta_0(s)}{\theta_c(s)} = \frac{K_1}{\frac{s^2}{\omega_1^2} + \frac{2\zeta_1 s}{\omega_1\left(\frac{s}{\omega_{RG}} + 1\right)} + 1} . \qquad (37)$$

These results indicate that with no feedback the short period characteristics are those of the free airframe defined by Equation 32. With a very large loop gain, these characteristics are defined by the roots of the equation

$$\frac{s^2}{\omega_1^2}\left(\frac{s}{\omega_{RG}} + 1\right) + \frac{2\zeta_1 s}{\omega_1} + \frac{s}{\omega_{RG}} + 1 = 0 \quad . \qquad (38)$$

The roots of Equation 38 are functions of the rate gyro dynamics; therefore, it is seen that even for an infinite loop gain the system does not attain the ideal characteristics. Since the ratio of the gyro characteristic frequency to the ideal short period frequency is of the order of 20 or 30, the short period roots of Equation 38 do not deviate markedly from the ideal roots. This is shown in Figure 10 by the variation in the terminal points of the loci.

In the midrange of values of loop gain, the system dynamics are represented by the roots of the equation

$$\left(\frac{s}{\omega_{RG}} + 1\right)\left(\frac{s^2}{\omega_0^2} + \frac{2\zeta_0 s}{\omega_0} + 1\right) + \frac{K_o K_2}{K_1}\left[\frac{s^2}{\omega_1^2}\left(\frac{s}{\omega_{RG}} + 1\right) + \frac{2\zeta_1 s}{\omega_1} + \frac{s}{\omega_{RG}} + 1\right] = 0. \qquad (39)$$

In Figure 10 the effect of loop gain is shown for two finite values of ω_{RG}, namely, 40 and 60 radians per second and an infinite characteristic frequency. The set of curves for which ω_{RG} is infinite represents the system with an ideal

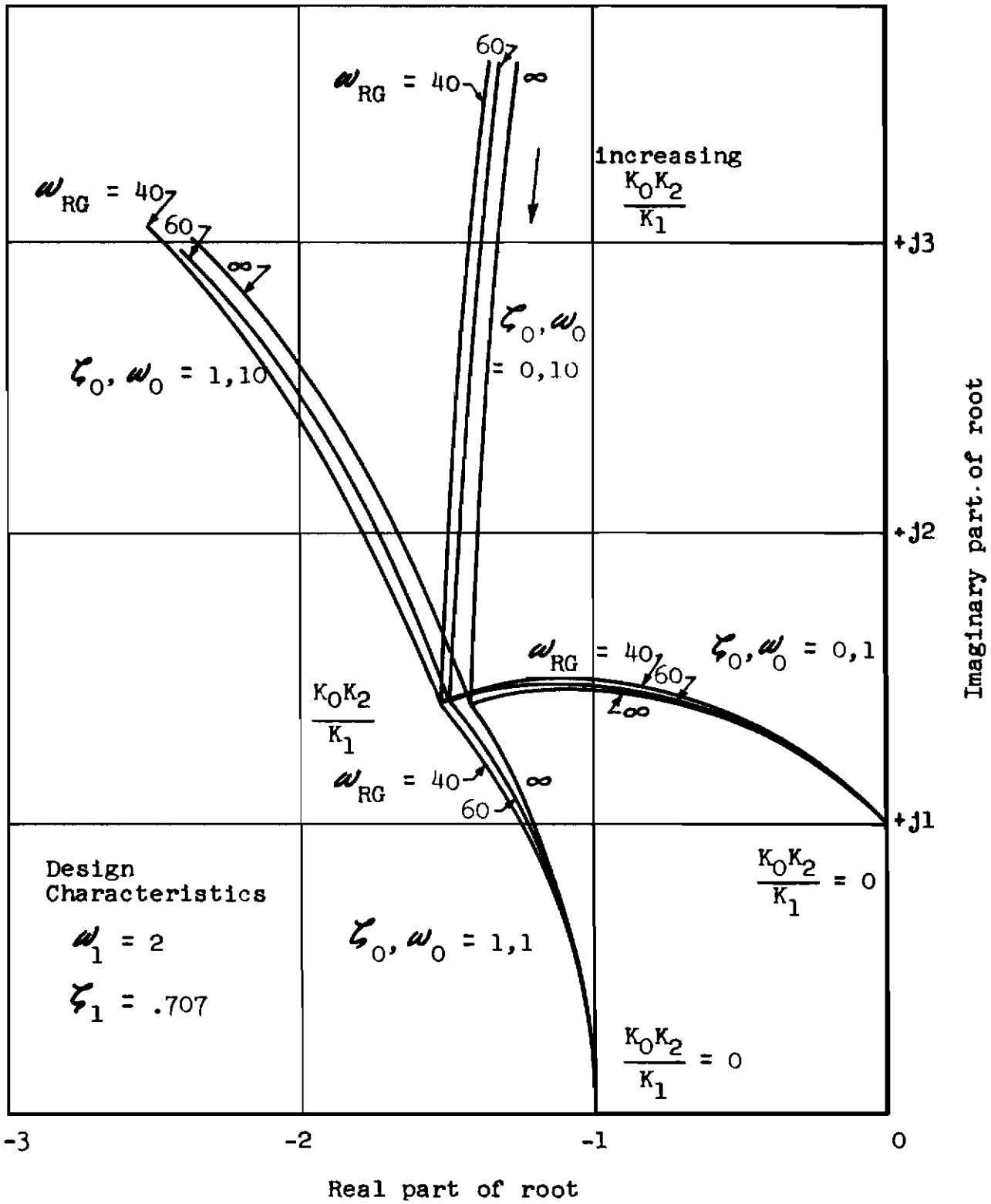

Fig. 10 EFFECT OF RATE GYRO ON CLOSED-LOOP, SHORT PERIOD CHARACTERISTICS FOR DIFFERENT LOOP GAINS AND FREE AIRFRAME CHARACTERISTICS

gyro. As the characteristic frequency of the gyro is decreased, the loci of the short period roots deviate further from the ideal case. In Figure 10 it is shown that these loci shift towards larger negative real parts as the gyro frequency decreases.

Effect of the Angular Accelerometer

The effects of the accelerometer alone (Fig. 11) are obtained from Equation 27 by omitting the hydraulic servodynamics and the rate gyro dynamics. This equation may then be written as follows:

$$\frac{\theta_0(s)}{\theta_C(s)} = \frac{K_1}{\left(\frac{s^2}{\omega_0^2} + \frac{2\zeta_0 s}{\omega_0} + 1\right) + \frac{K_o K_2}{K_1}\left[\frac{s^2}{\omega_1^2\left(\frac{s^2}{\omega_A^2} + \frac{2\zeta_A s}{\omega_A} + 1\right)} + \frac{2\zeta_1 s}{\omega_1} + 1\right]}. \quad (40)$$

As $\frac{K_o K_2}{K_1}$ approaches zero, Equation 40 approaches

$$\frac{\theta_0(s)}{\theta_C(s)} = \frac{K_o K_2}{\frac{s^2}{\omega_0^2} + \frac{2\zeta_0 s}{\omega_0} + 1}. \quad (41)$$

As $\frac{K_o K_2}{K_1}$ approaches infinity, Equation 40 approaches

$$\frac{\theta_0(s)}{\theta_C(s)} = \frac{K_1}{\frac{s^2}{\omega_1^2\left(\frac{s^2}{\omega_A^2} + \frac{2\zeta_A s}{\omega_A} + 1\right)} + \frac{2\zeta_1 s}{\omega_1} + 1}. \quad (42)$$

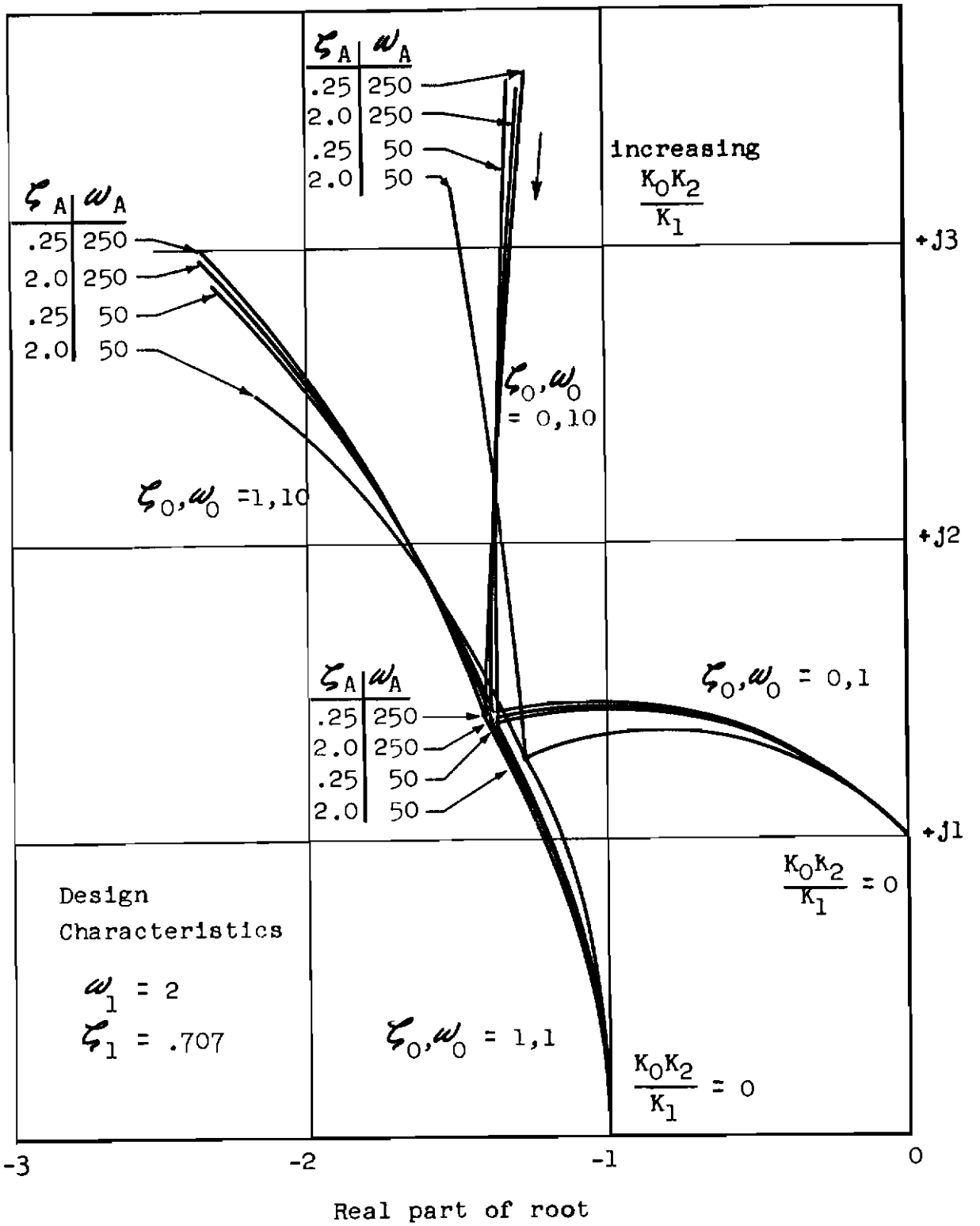

Fig. 11 EFFECT OF ACCELEROMETER ON CLOSED-LOOP, SHORT PERIOD CHARACTERISTICS FOR DIFFERENT LOOP GAINS AND FREE AIRFRAME CHARACTERISTICS

With no feedback, the short period characteristics are equal to those of the free airframe. With a very large feedback gain, these characteristics are defined by the roots of the equation

$$\frac{s^2}{\omega_1^2} + \left(\frac{s^2}{\omega_A^2} + \frac{2\zeta_A s}{\omega_A} + 1\right)\left(\frac{2\zeta_1 s}{\omega_1} + 1\right) = 0. \qquad (43)$$

The short period roots of Equation 43 are functions of the natural frequency and damping ratio of the accelerometer; therefore, the system does not attain the ideal characteristics even for an infinite loop gain. In the range of ratios of accelerometer natural frequency to short period frequency, of the order of 25 to 125, the effect of accelerometer dynamics at very large feedback gains is very small. The greatest deviation of the terminal point from the ideal point occurs for accelerometer characteristics of $\omega_A = 50$ radians per second and $\zeta_A = 2.0$. These results are illustrated graphically by the terminal points of the loci in Figure 11. In the midrange of values of loop gain, the system dynamics are represented by the roots of the equation

$$\left(\frac{s^2}{\omega_0^2} + \frac{2\zeta_0 s}{\omega_0} + 1\right)\left(\frac{s^2}{\omega_A^2} + \frac{2\zeta_A s}{\omega_A} + 1\right) + \frac{K_0 K_2}{K_1}\left[\frac{s^2}{\omega_1^2} + \left(\frac{2\zeta_1 s}{\omega_1} + 1\right)\left(\frac{s^2}{\omega_A^2} + \frac{2\zeta_A s}{\omega_A} + 1\right)\right] = 0. \qquad (44)$$

In Figure 11 the effect of loop gain, $\frac{K_0 K_2}{K_1}$ on the short period roots of Equation 44 is shown for four combinations of accelerometer natural frequency and damping ratio as follows

ω_A	ζ_A
50	0.25
50	2.0
250	0.25
250	2.0

The distortion of the loci from that of the ideal case is small except for the case $\omega_A = 50$ and $\zeta_A = 2.0$. In this instance the loci terminal point appears to be shifted towards the origin in relation to the ideal terminal point. This indicates a reduction in the short period frequency which is attained with little change in damping ratio.

The shifts of the root loci and the deviation of the terminal points of these loci from the design value resulting from the accelerometer and the rate gyro dynamics may be utilized to the designer's advantage. The use of these phenomena in the synthesis of the system will be discussed in the following section.

Effects of Added Components on System Stability

The closed-loop short period natural frequency and damping ratio that are produced by the self-adaptive control system previously discussed have been shown to vary significantly with changes in loop gain but to vary only slightly in terms of variations in sensor and servodynamics. The realistic system shown in Figure 7 contains components which generate additional modes of motion that are superimposed upon the short period motion. The interaction between these additional modes and the short period mode is evident in Figures 9, 10, and 11 and is shown by the displacement of the short period roots. The actual roots which caused these displacements are not shown in Figures 9, 10, and 11. They become important only when their real parts approach positive values indicating system instability.

Stability problems resulting from these additional components may be studied by conventional methods of analysis in which Root Locus, Bode, or Nyquist diagrams are used. The application of any one of these three methods to the multiple loop control system previously discussed would be tedious and mathematically complicated because the effects of changes in component dynamics and feedback gains enter into all three of the feedback loops. The most desirable analytical technique is that which requires the least recalculation when any of the above parameters are varied. For this reason a relatively new technique, the dual Nyquist method, was selected at most applicable on this analysis.

Derivation of the Dual Nyquist Diagram

The dual Nyquist diagram is a graphical procedure for determining the stability of feedback systems. A mathematical derivation of this technique is described in Reference 2; a short introduction to the method is included in Appendix A. The particular application of this method to the present problem may be approached by representing the closed-loop transfer of the system in several ways. The approach which was chosen separates the forward path of the loop from the feedback path which in turn separates the effects carried by sensor dynamics from those caused by airframe and hydraulic servodynamics.

The complete closed-loop transfer function, Equation 23, may be written as follows:

$$\frac{\theta_0(s)}{\theta_C(s)} = \frac{K_1}{\frac{K_1}{K_0K_2}\left(\frac{s}{\omega_{HS}}+1\right)\left(\frac{s^2}{\omega_0{}^2}+\frac{2\zeta_0 s}{\omega_0}+1\right)\left[\frac{s^2}{\omega_1{}^2\left(\frac{s^2}{\omega_A{}^2}+\frac{2\zeta_A s}{\omega_A}+1\right)}+\frac{2\zeta_1 s}{\omega_1\left(\frac{s}{\omega_{RG}}+1\right)}+1\right]} \quad (45)$$

or

$$\frac{\theta_0(s)}{\theta_C(s)} = \frac{K_1}{A(s)+B(s)}$$

where

$$A(s) = \frac{K_1}{K_0K_2}\left(\frac{s}{\omega_{HS}}+1\right)\left(\frac{s^2}{\omega_0{}^2}+\frac{2\zeta_0 s}{\omega_0}+1\right) \quad (46)$$

and

$$B(s) = \frac{s^2}{\omega_1{}^2\left(\frac{s^2}{\omega_A{}^2}+\frac{2\zeta_A s}{\omega_A}+1\right)}+\frac{2\zeta_1 s}{\omega_1\left(\frac{s}{\omega_{RG}}+1\right)}+1. \quad (47)$$

It should be noted that the forward path transfer function is equal to $\frac{K_1}{A(s)}$ and that the feedback path transfer function is equal to $\frac{B(s)}{K_1}$. A change in flight condition or servodynamics affects only A(s), and a change in sensor dynamics affects only B(s).

In order to apply the dual Nyquist theory, the maps of the complex functions A(s) and B(s) must be plotted as the complex variable s traces out a contour enclosing the right half of the complex plane. The general shapes of these loci may be approximated by considering the five significant values of the variable s, as follows:

$$s = 0 + j0$$

$$s = 0 + j\omega_1, \quad 0 < \omega_1 < \infty$$

$$s = 0 + j\infty$$

$$s = \infty + j\infty$$

$$s = \infty + j0.$$

A sketch of the location of these five points on the complex plane is shown in Figure 12. The numbers on this curve locate the particular points selected above. In Figure 12 is shown only that part of the contour in the first quadrant of the complex plane.

The shape of the plots of A(s) and B(s), as s traces this contour, are shown in Figures 13 and 14, respectively. The numbers on these curves correspond to those in Figure 12. These figures are maps of the functions A(s) and B(s) as s traces that part of the contour in the first quadrant of the complex plane. To complete the dual Nyquist plot, the fourth quadrant must be plotted. By reflecting each of the curves into the axis, the complete figures are obtained.

By applying the dual Nyquist procedures as explained in Appendix A, the functions A(s) and -B(s) must be plotted simultaneously, and their points of intersection examined. A general sketch of the dual Nyquist diagram is shown in Figure 15. In order for the over-all system to be stable, the frequency on the locus of A(s) at the point of intersection must be less than that on the locus of -B(s) at the point of intersection.

Since neutral stability occurs when the two curves intersect at the same frequency, it is evident that the relative values of frequencies at the intersection provides at least a qualitative measure of system stability.

Stability Considerations in the Synthesis of the Final Control System

The vehicle to which the dual Nyquist method of stability analysis was applied consisted of an air-to-surface powered supersonic missile of a type originally considered for use in conjunction with a supersonic bomber. For the purpose of making this stability analysis, it is not necessary to know all of the usual aerodynamic data. It is

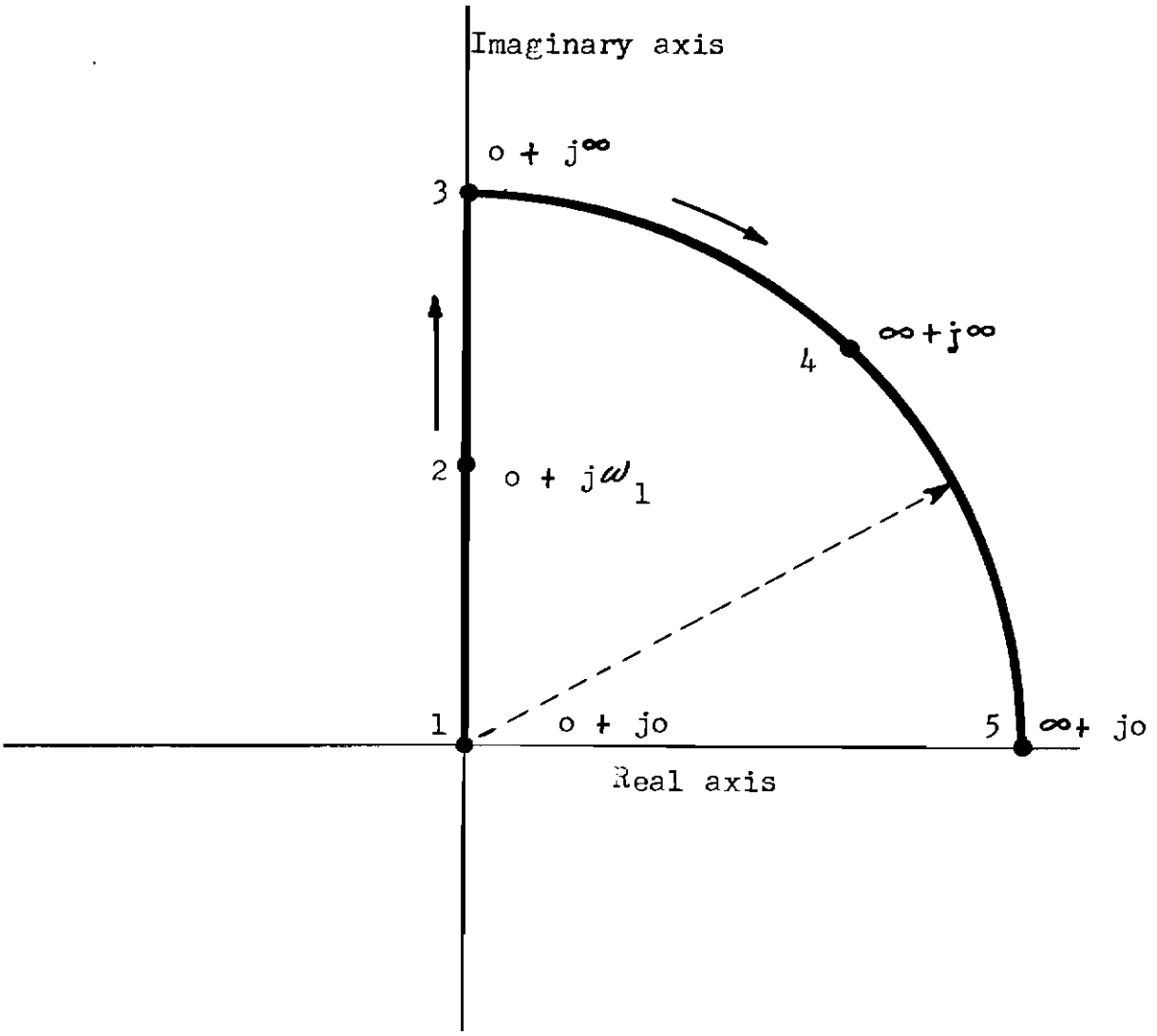

Fig. 12 CONTOUR ON COMPLEX PLANE ENCLOSING THE RIGHT HALF PLANE

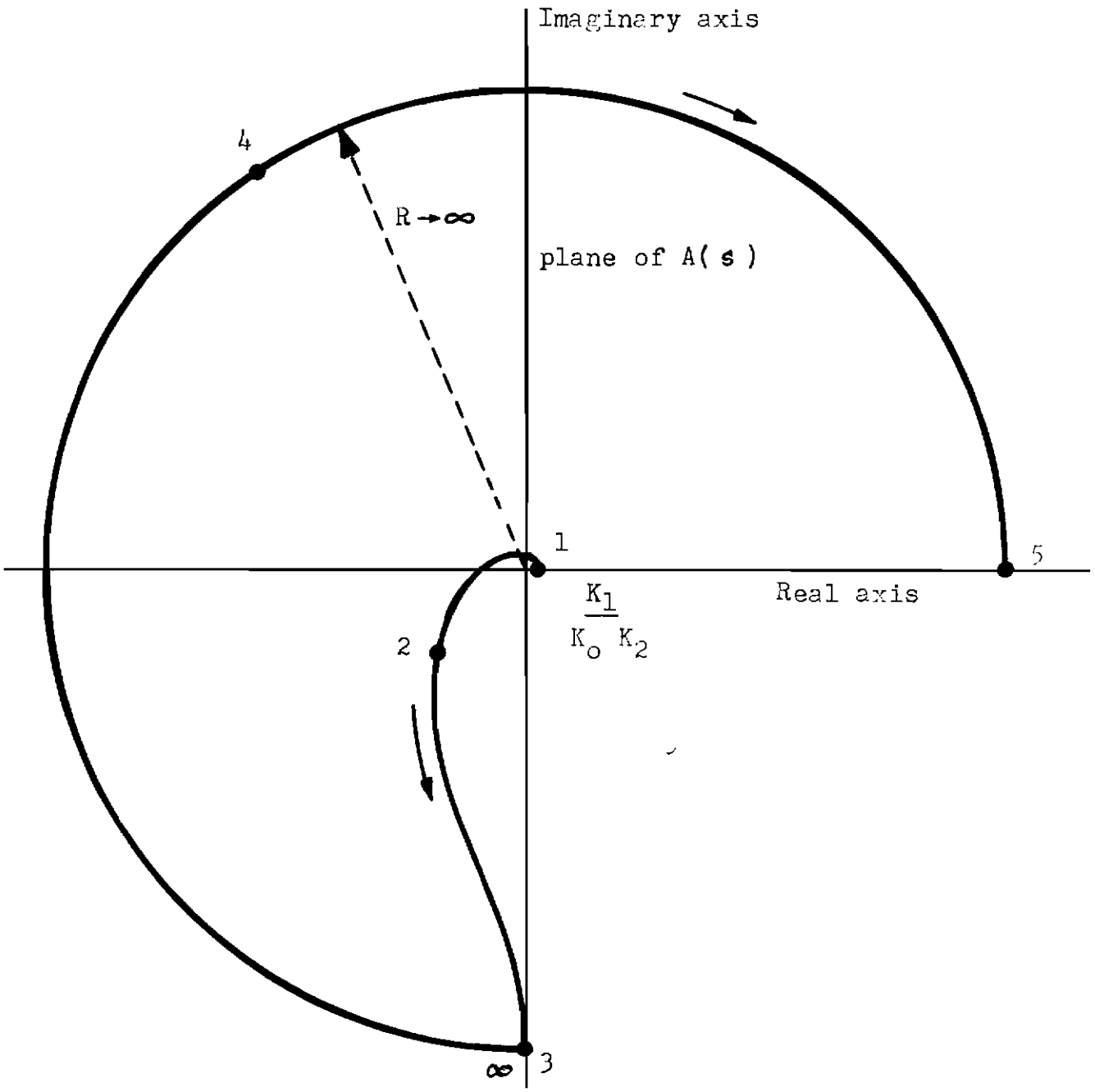

Fig. 13 MAP OF FUNCTION A(s) ON COMPLEX PLANE

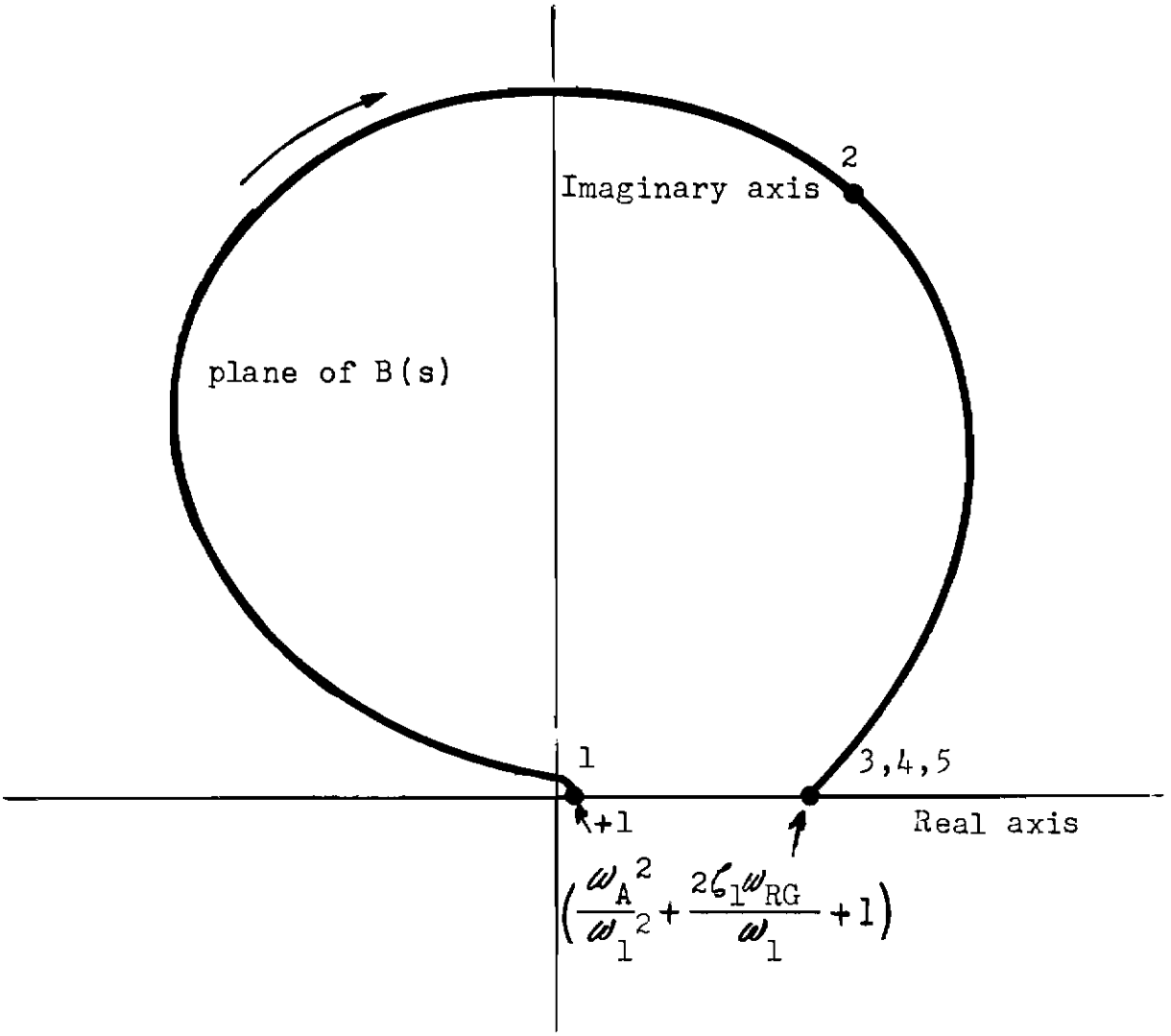

Fig. 14 MAP OF FUNCTION B(s) ON COMPLEX PLANE

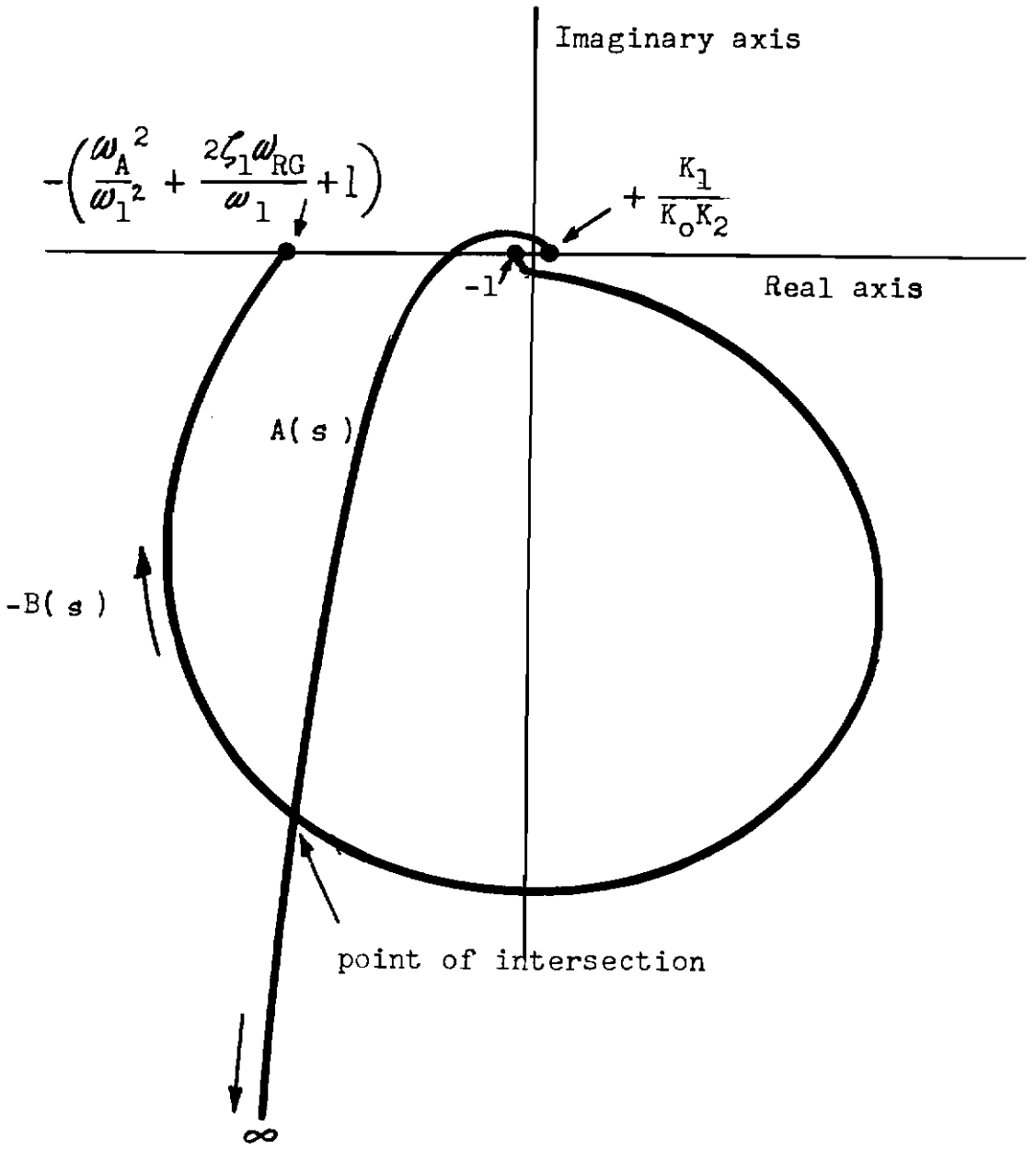

Fig. 15 DUAL NYQUIST DIAGRAM

necessary to determine only the extremes in undamped natural frequency, steady state gain, and damping ratio of the free airframe. The first two are important in determining both the over-all system performance and the gain limitations for stability. The last, damping ratio, is important only as a limiting factor in obtaining optimum performance, and, as will be illustrated, large changes in damping ratio do not complicate the stability problem to any considerable degree.

Table I contains the values of the significant parameters at each of three flight conditions which were chosen for illustration.

TABLE I

FREE AIRFRAME SHORT PERIOD CHARACTERISTICS
AT ILLUSTRATIVE FLIGHT CONDITIONS

Condition	Steady Stage Gain, K_o	Undamped Natural Frequency, ω_0	Damping Ratio, ω_0
1	5.7	1.1	0.05
2	2.69	2.8	0.20
3	1.016	4.84	0.30

The range of frequency and damping which are represented is typical of a large number of modern aircraft so that the values chosen constitute a good illustration for a self-adaptive control synthesis.

Effect of Flight Condition Upon Stability - Figure 16 is a diagram containing graphs of the loci of the functions A(s) and -B(s) defined previously in Equations 46 and 47. The locus of A(s) depends upon flight condition, control loop gain, and hydraulic servodynamics. Three curves are shown corresponding to the flight conditions listed in Table I. The gain factor, K_2/K_1, was assumed equal to unity to facilitate computation and the hydraulic servo characteristic frequency, ω_{HS}, was assumed to be 20 radians per second. The locus of -B(s) depends upon rate gyro and accelerometer dynamics and upon the desired closed-loop system short period characteristics. The assumed rate

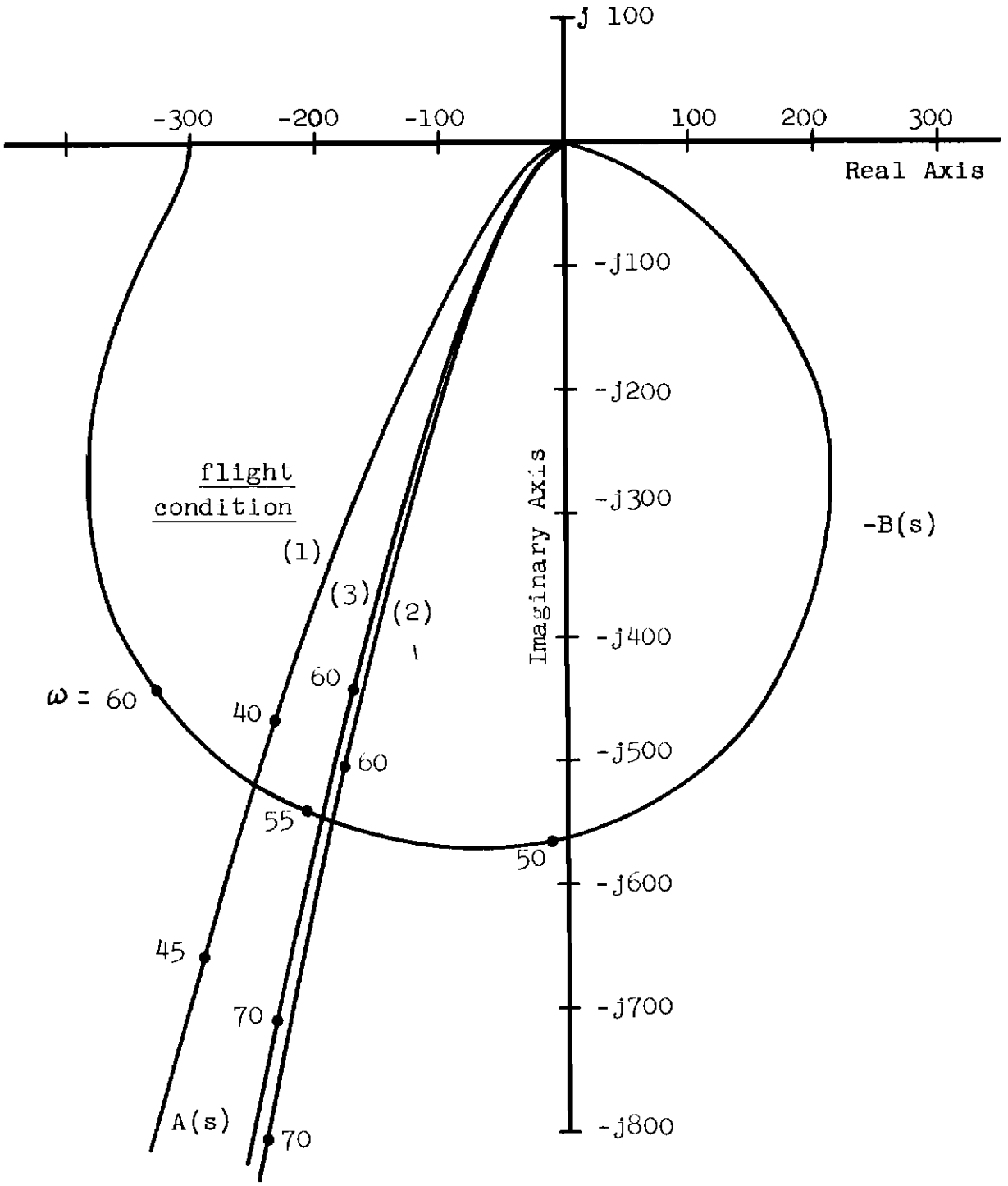

Fig. 16 DUAL NYQUIST DIAGRAM SHOWING EFFECT OF FLIGHT CONDITION UPON STABILITY

gyro characteristic frequency was ω_{RG} = 40 radians per second. The accelerometer characteristics were ω_A = 50 radians per second and ζ_A = 0.25. The component characteristics chosen for this illustration correspond to the lowest values of frequency and damping ratio in the range of component parameters previously used in this report. The desired short period characteristics were ω_1 = 3.0 radians per second and ζ_1 = 0.707. These were chosen within the "good" range of pilot's preference ratings shown in Reference 3. This range lies between natural frequencies of 2 to 4 radians per second and damping ratios of 0.45 to 1.0. These values represent the desired limits for manned aircraft. For pilotless aircraft other design points may be more desirable from the point of view of structural limitations, range, altitude, speed, performance, accuracy, and other operational considerations.

It is seen by inspection of Figure 16 that for the gain, K_1/K_2, equal to unity, the frequency on the curve representing A(s) at the point of intersection is lower than that corresponding to B(s) for condition (1) and higher for conditions (2) and (3). Therefore, the system is stable at condition (1) and unstable at conditions (2) and (3). The condition for which instability is the greatest is condition (3). This is to be expected since at condition (3) occurs the highest natural frequency, closest to the component frequencies.

Effect of Loop Gain Upon System Stability - Because of the manner in which the system transfer function was written in order to develop the dual Nyquist diagram, the reciprocal of the gain factor, K_1/K_2, appears as a term in the over-all system loop gain. The system loop gain is $\frac{K_2K_o}{K_1}$ (see Fig. 7). Thus, if the over-all loop gain is reduced sufficiently, by increasing the factor K_1/K_2, to stabilize the system response at the least stable condition (condition (3)), this value of gain will also produce a stable response at the other conditions shown in Table I.

A simple graphical method of computing the loop gain required to produce neutral stability is shown in Figure 17. The solid curves are identical to the curves representing flight condition (3) and -B(s) in Figure 16. As can be seen, a vector has been drawn from the origin through the point ω = 55.5 radians per second on the curve A(s). This vector also intersects the curve -B(s) at the point ω = 55.5 radians per second. This is the only frequency at which such an intersection is possible. It is the neutral stability frequency.

The vector which determines the neutral stability frequency may be found graphically by trial and error. In Figure 17 the vector distance from the origin to the curve A(s) was increased by a factor of 1.587. Therefore the loop gain at neutral stability for condition (3) must be

$$\frac{K_2K_o}{K_1} = \frac{1}{1.587} \cdot 1.016 = 0.64 . \qquad (48)$$

The dashed line in Figure 17 represents a locus of the curve of A(s) at condition (3) for this new loop gain. It is shown merely for illustration and is not necessary in the determination of the proper gains.

The loop gains obtained at the other two flight conditions by increasing the factor K_1/K_2 to 1.587 are calculated as follows. For condition (2)

$$\frac{K_oK_2}{K_1} = \frac{2.69}{1.587} = 1.695 \qquad (49)$$

and for condition (1),

$$\frac{K_oK_2}{K_1} = \frac{5.7}{1.587} = 3.59. \qquad (50)$$

The gain margins for conditions (1) and (2) for these loop gains become 3.42 and 1.123, respectively.

A method was described above for determining the loop gain for neutral stability at one flight condition. It appears that a gain margin of 1.414 (3 db.) is sufficient for the system described in this report. The choice of gain margin depends, of course, upon the accuracy of measurement of system parameters and variations of component dynamics resulting from environmental changes. In the self-adaptive system which is discussed it is best not to overdesign because a reduction in loop gain causes the system characteristics to depart from the ideal characteristics.

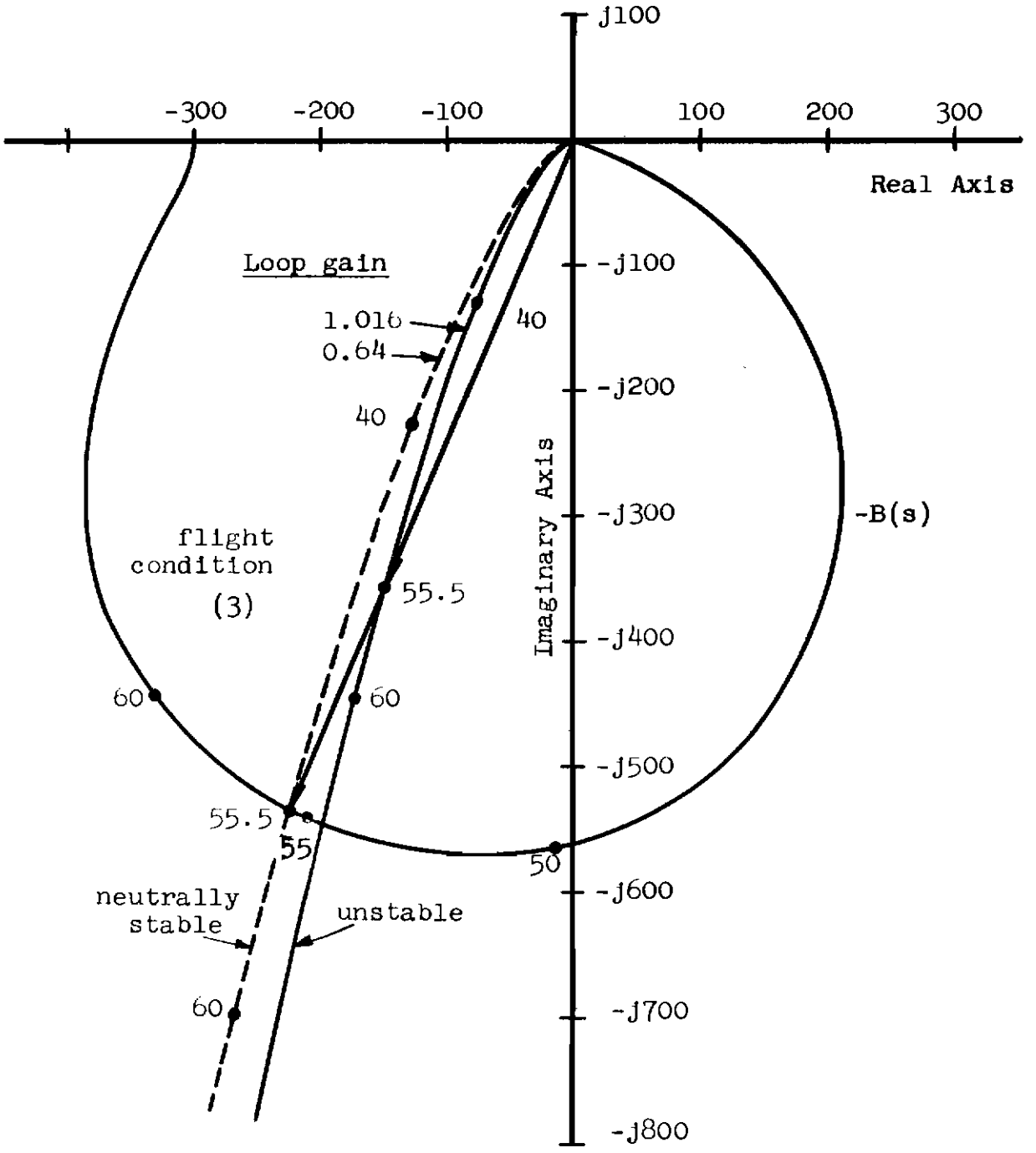

Fig. 17 DUAL NYQUIST DIAGRAM SHOWING EFFECT OF LOOP GAIN UPON STABILITY

Effect of Hydraulic Servo Characteristic Frequency Upon System Stability - Figure 18 represents a dual Nyquist diagram which shows the effect of a change in servo characteristics. Two values of servo characteristic frequency are shown at each of the three flight conditions listed in Table I. They are ω_{HS} = 20 radians per second and ω_{HS} = 50 radians per second. The curves which represent a servo frequency of 20 radians per second are identically the same as those shown in Figure 16. The additional curves representing a frequency of 50 radians per second show an unexpected phenomenon: an increase in servo frequency causes the system to become less stable. For example, in order to bring the response at condition (3), with ω_{HS} = 50 (the least stable) to neutral stability, the loop gain must be reduced by a factor of 2.07 instead of only 1.587 with ω_{HS}= 20.

The term $\left(\frac{s}{\omega_{HS}} + 1\right)$ in Equation 46 at any particular value of $s = j\omega$, has less phase lead and has less magnitude when ω_{HS} = 50 than when ω_{HS} = 20. The first effect, that of producing less phase lead when ω_{HS} = 50, results in a shift of the curve of A(s) in the clockwise direction around the origin. This causes the locus of A(s) to cross the locus of B(s) at a higher frequency point on the locus of B(s) which, taken alone, implies an improvement in stability. The second effect, that of decreasing magnitude, results in an increase in the frequency on the locus of A(s) at the point of intersection which, taken alone, implies a decrease in stability.

In the range of servo frequencies which are of interest in this problem, the decreased gain more than compensates for the decreased phase lead, and, as a result, the system becomes less stable. At frequencies above the range of interest, the reverse compensation takes place, and the system becomes more stable again.

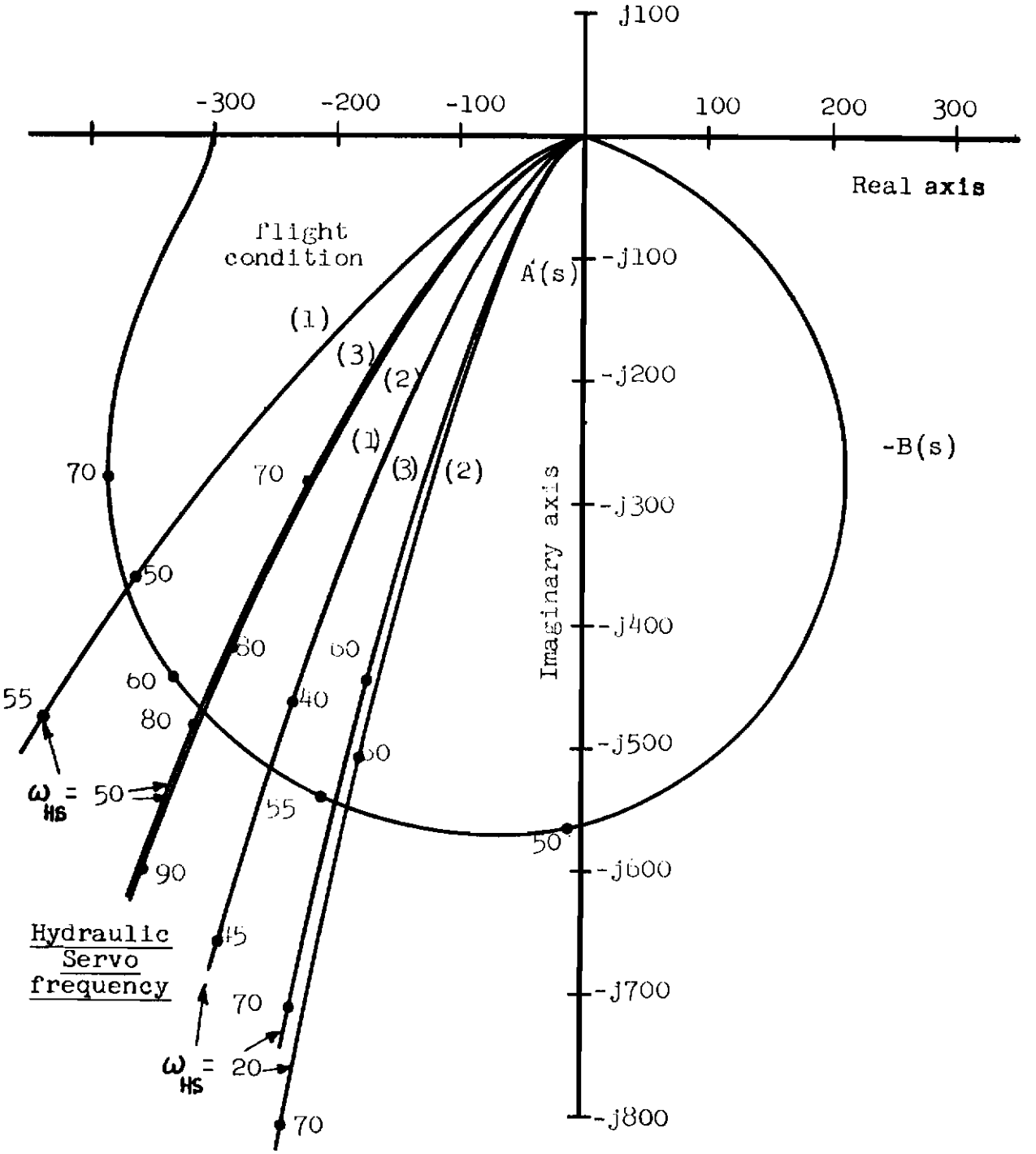

Fig. 18 DUAL NYQUIST DIAGRAM SHOWING EFFECT OF HYDRAULIC SERVO UPON STABILITY

Effect of Rate Gyro Characteristic Frequency Upon System Stability - Figure 19 represents a dual Nyquist diagram which shows the effect of a change in rate gyro characteristics. Two values of rate gyro characteristic frequency are represented: ω_{RG} = 40 radians per second and ω_{RG} = 60 radians per second. These effects appear as changes in the locus of -B(s) and are very small. The three loci of A(s) represent the three flight conditions mentioned previously and are identical with the corresponding curves in Figure 16.

An increase in rate gyro frequency causes the locus of -B(s) to expand radially away from the origin. As a result the frequency at the point of intersection on the locus of A(s) increases. This effect implies a decrease in stability. The above effect is easily proved to be small by expressing Equation 47 in the following form

$$B(s) = \frac{\left(\frac{s}{\omega_p} + 1\right)\left(\frac{s^2}{\omega_q^2} + \frac{2\zeta_q s}{\omega_q} + 1\right)}{\left(\frac{s}{\omega_{RG}} + 1\right)\left(\frac{s^2}{\omega_A^2} + \frac{2\zeta_A s}{\omega_A} + 1\right)} . \qquad (51)$$

By using this form, it can be shown that

$$\zeta_q \approx \zeta_1 = .707,$$

$$\omega_q \approx \omega_1 = 3.0,$$

$$\omega_p \approx \omega_{RG},$$

and

$$\omega_{RG} - \omega_p \approx 2\zeta_q \omega_q \approx 4.242.$$

Thus in the range of usable rate gyro frequencies (ω_{RG} = 40 to 60), ω_p and ω_{RG} differ by at most about 10 percent of their value. As a result the term $\left(\frac{s}{\omega_p} + 1\right)$ in the numerator

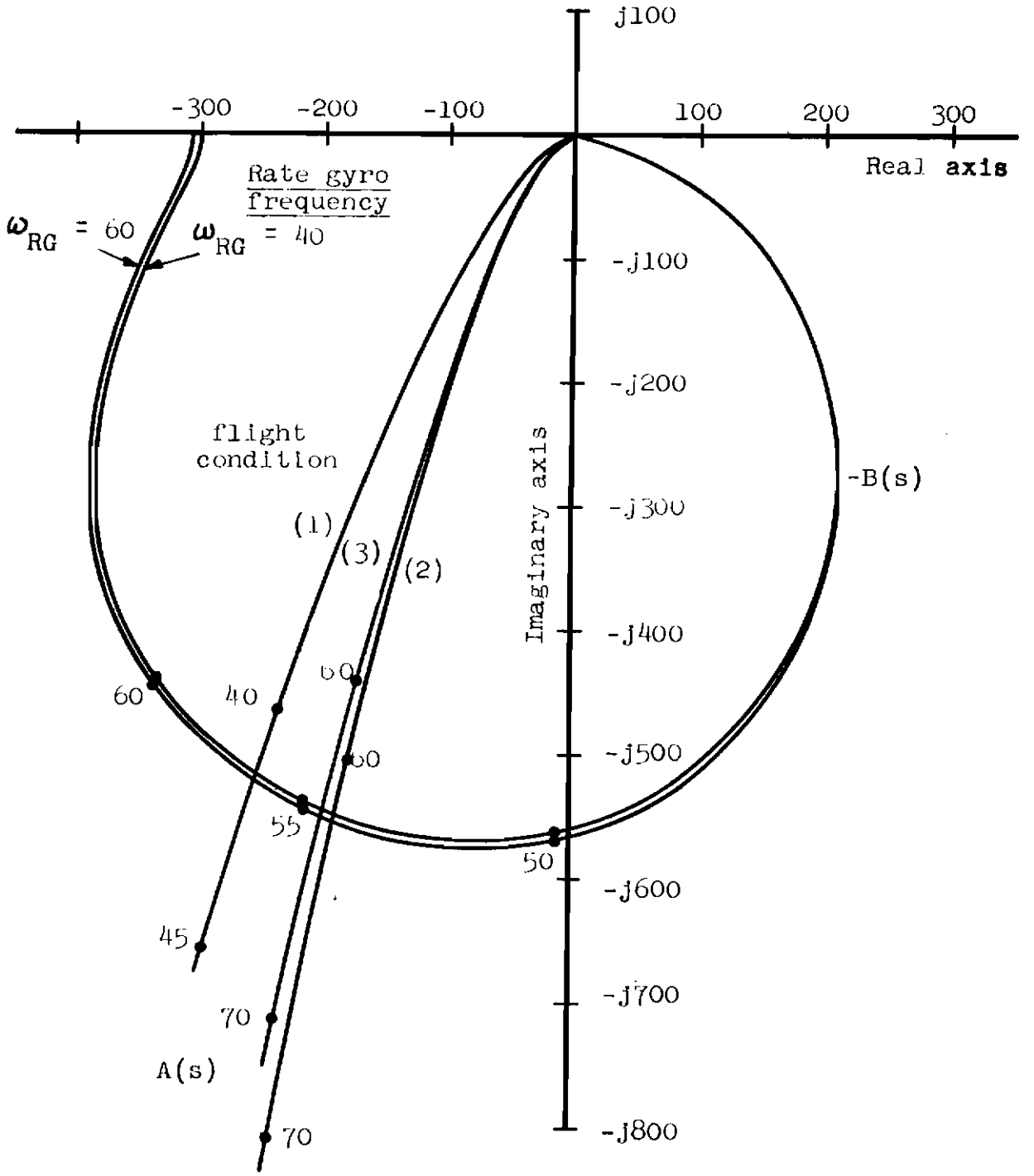

Fig. 19 DUAL NYQUIST DIAGRAM SHOWING EFFECT OF RATE GYRO UPON STABILITY

of Equation 51 almost exactly cancels the term $\left(\frac{s}{\omega_{RG}} + 1\right)$ in the denominator. Consequently, a significant change in stability resulting from a variation in ω_{RG} would hardly be expected. As a first approximation then, the locus of B(s) may be computed from

$$B(s) \approx \frac{\frac{s^2}{\omega_1^2} + \frac{2\zeta_1 s}{\omega_1} + 1}{\frac{s^2}{\omega_A^2} + \frac{2\zeta_A s}{\omega_A} + 1} \cdot \qquad (52)$$

It has been mentioned previously that there is no significant change in the effects of rate gyro dynamics on system stability whether these dynamics are represented by a first order transfer function, as has been assumed in this analysis, or by a second order system with typical characteristics $\zeta_{RG} = 0.7$ and $\omega_{RG} = 100$. This unappreciable effect on system stability is easily shown by examining the true expression for B(s), Equation 47. Only the second term contains the rate gyro characteristics and it varies with s to the first power. The first term varies with s to the second power; therefore, it becomes far more significant than the second term at large values of s. For this reason alone variations in rate gyro dynamics will not cause significant changes in B(s) at large values of s. The difference in effect on B(s), between use of the second order rate gyro representation mentioned above and use of the first order representation considered throughout the analysis, was computed. Results of this comparison are listed below:

B(s)	First order rate gyro $\omega_{RG} = 40$	Second order rate gyro $\zeta_{RG} = .7$, $\omega_{RG} = 100$
at s = j50	12.4 + j564	16.6 + j572
s = j60	331 + j442	336 + j453
s = j100	350 + j118	367 + j111

Reference to Figure 19 shows that the above variations between first and second order representations are insignificant and are approximately equal to the variations between a first order system with $\omega_{RG} = 40$ and $\omega_{RG} = 60$.

Effect of Accelerometer Undamped Natural Frequency Upon System Stability - Figure 20 represents a dual Nyquist diagram which shows the effect of a change in accelerometer undamped natural frequency. Two values of accelerometer frequency are represented: $\omega_A = 50$ radians per second and $\omega_A = 250$ radians per second. The curves representing the loci of A(s) and the locus of -B(s) for $\omega_A = 50$ radians per second are identical to the curves plotted in Figure 16.

An increase in accelerometer frequency, with no change in accelerometer damping ratio, ζ_A, causes the locus of -B(s) to expand about the origin. This expansion does not decrease stability as occurred in the case of an increase in rate gyro frequency because the frequency points are shifted along the locus of -B(s) in a counterclockwise direction as ω_A is increased. The general result is an increase in stability with increasing accelerometer frequency.

As a first approximation, it was shown that the effects of rate gyro characteristic frequency may be neglected. As a result, the function B(s) was approximated by a ratio of two quadratic polynomials in s as shown by Equation 52.

Since ω_A is much greater than ω_1, the phase angles of the numerator of Equation 52 are almost + 180 degrees for frequencies that are greater than or equal to ω_A. Hence the phase angle of -B(s) is approximately equal to - [180 degrees - phase angle of denominator, Equation 52] for all values of frequency that are greater than or equal to ω_A.

Figure 20 reveals that the phase angle of the locus of -B(s) for $\omega_A = 50$ radians per second at a frequency equal to an arbitrary fixed multiple (greater than or equal to unity) of 50 radians per second is almost identically the same as the phase angle of the locus of -B(s) for $\omega_A = 250$ radians per second at a frequency equal to the same multiple of 250 radians per second. This observation may be written concisely as follows

$$\text{phase of } \left[-B(s)_{\omega_A=50}\right]_{\omega=50K} \approx \text{phase of } \left[-B(s)_{\omega_A=250}\right]_{\omega=250K} \tag{53}$$

where K is an arbitrary multiplier.

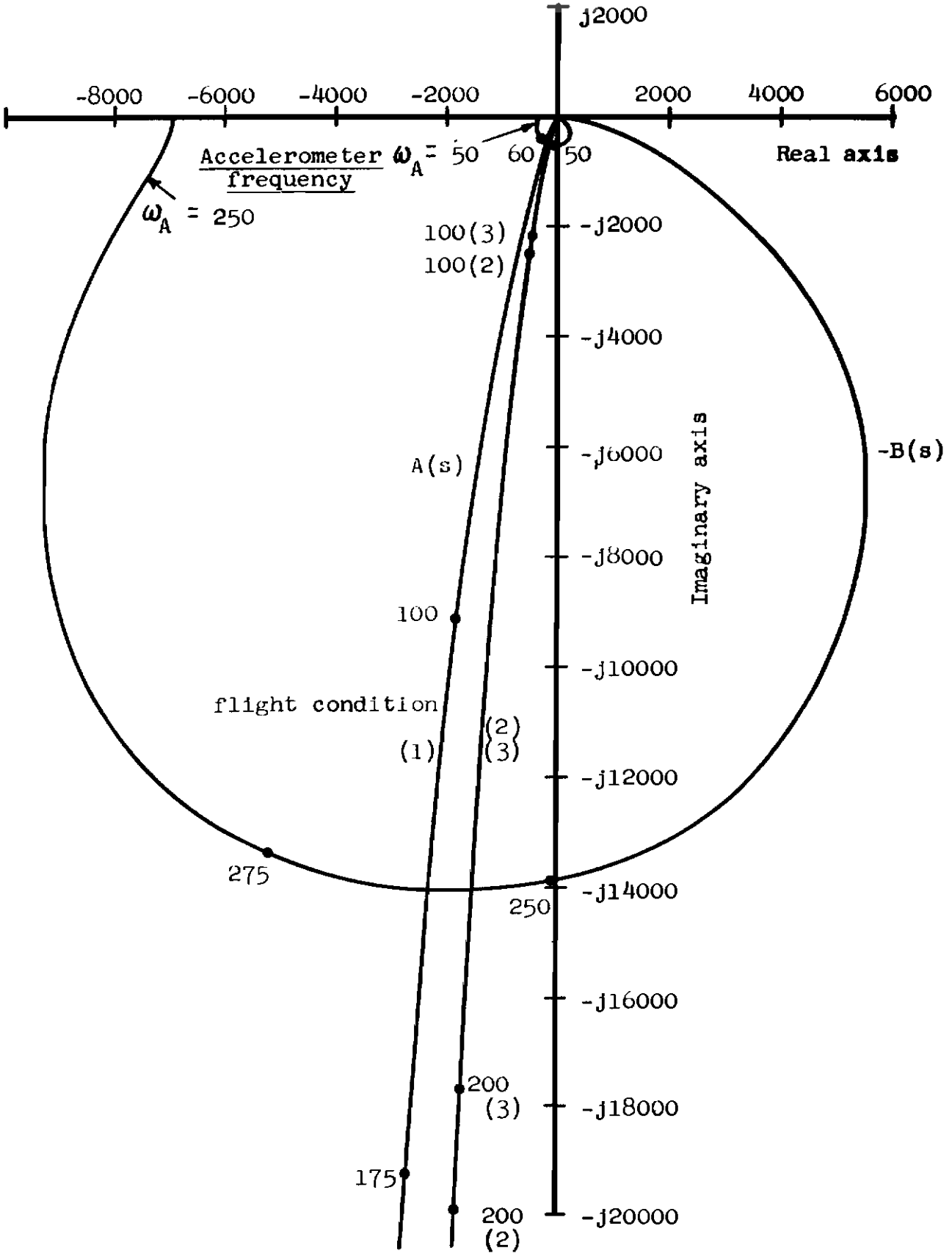

Fig. 20 DUAL NYQUIST DIAGRAM SHOWING EFFECT OF ACCELEROMETER UNDAMPED NATURAL FREQUENCY UPON STABILITY

Inspection of Equation 52 reveals that the magnitudes of the loci of -B(s) (i.e., the vector distances from the origin to the loci of -B(s) shown in Fig. 20) are related as follows for frequencies that are greater than or equal to ω_A.

$$\frac{\left|-B(s)_{\omega_A=50}\right|_{\omega=50K}}{\left|B(s)_{\omega_A=50}\right|_{\omega=250K}} = \frac{(50K)^2}{(250K)^2} = \left(\frac{50}{250}\right)^2 \quad (54)$$

Thus, from Equation 53, it is seen that, when a straight line is drawn from the origin intersecting the two loci of -B(s), the frequencies at the points of intersection on the loci of -B(s) are near identical multiples of the respective values of ω_A. Also, it is seen from Equation 54 that the ratio of the magnitudes of the above distance from the origin to each point of intersection is equal to the square of the ratio of the respective values of ω_A.

From an inspection of Figure 20 it is evident that the phase angle of the locus of A(s) changes very slightly between the point where it intersects the locus of -B(s) for ω_A = 50 radians per second and the locus of -B(s) for ω_A=250 radians per second. Thus the approximation may be made that the locus of A(s) is almost a straight line from the origin. By referring to Equation 46, it can be seen that the magnitude of A(s) increases as the cube of the frequency for sufficiently large frequencies.

On the basis of the observations stated in the previous two paragraphs, it is therefore deduced that, as ω_A is increased, the intersection frequency on the locus of -B(s) becomes larger at a faster rate than the intersection frequency on the locus of A(s). Hence the system becomes more stable as ω_A is increased.

Effect of Accelerometer Damping-Ratio Upon System Stability - Figure 21 represents a dual Nyquist diagram which shows the effect of a change in accelerometer damping ratio. Two values of damping ratio are represented: ζ_A= .25 and ζ_A = 2.0. The curves representing the loci of A(s) and the locus of -B(s) for ζ_A = .25 are identical to the curves in Figure 16.

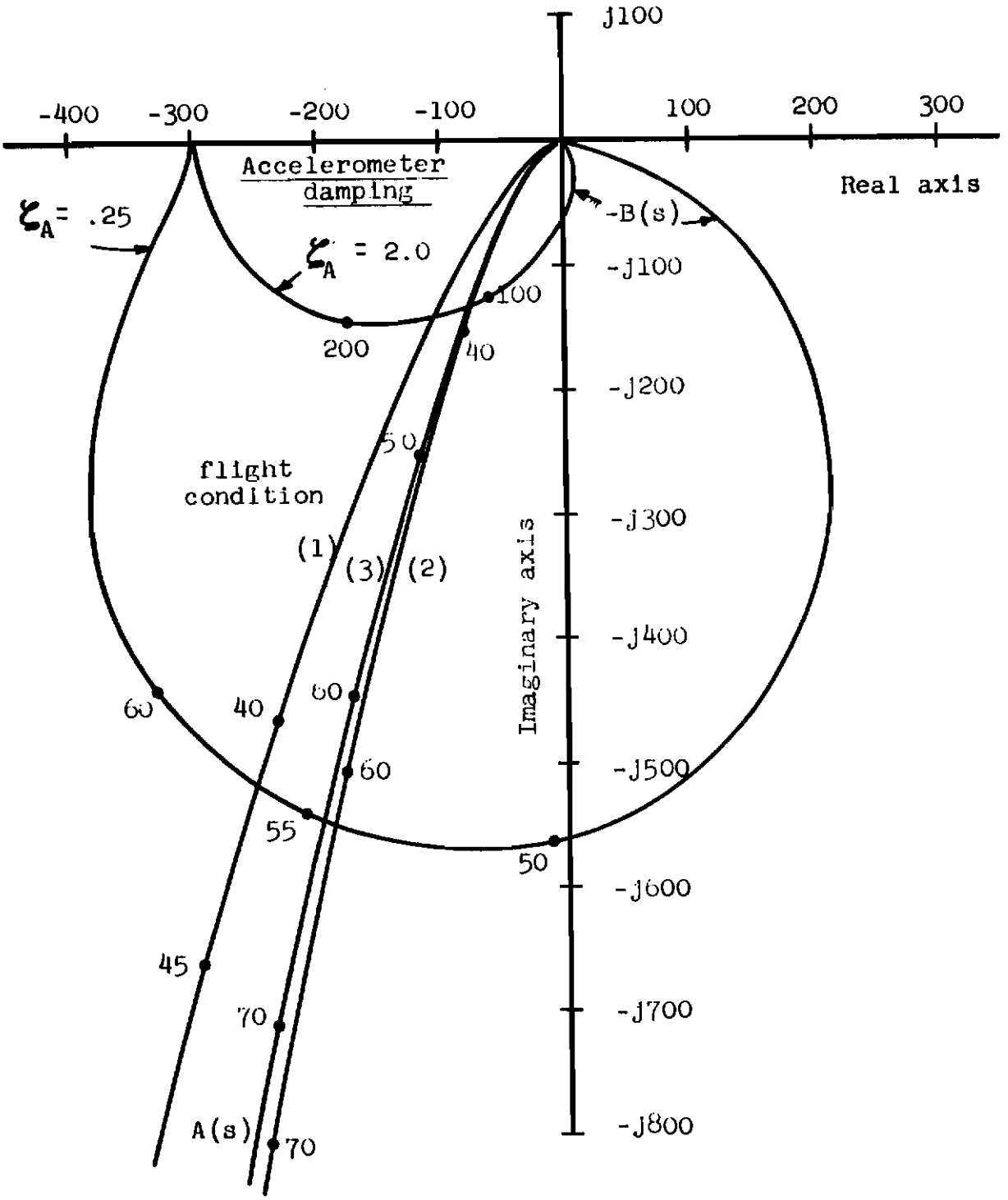

Fig. 21 DUAL NYQUIST DIAGRAM SHOWING EFFECT OF ACCELEROMETER DAMPING-RATIO UPON STABILITY

An increase in accelerometer damping ratio decreases the magnitude of the resonant peak of -B(s); consequently, the locus of -B(s) shrinks toward the origin as ζ_A is increased. This shrinking in itself implies an increase in stability since the locus of -B(s) crosses the locus of A(s) at a lower frequency on the locus of A(s). An increase in ζ_A also causes a decrease in phase lag of -B(s) at frequencies greater than ω_A. As a result, the frequency points are shifted along the loci of -B(s) in a counterclockwise direction which further increases stability. The total result is a considerable increase in stability with increasing accelerometer damping ratio.

Effect of Design Short Period Damping Ratio Upon System Stability - Although the design damping ratio, ζ_1, and natural frequency, ω_1, are not characteristics of components in the system, in Reference 3 it is indicated that there is some tolerable variation of these parameters. Therefore, although there may be a unique optimum design point, there appears to be enough acceptable variation in this point so that consideration ought to be given to the effect of variation in the design point upon the stability of the over-all system. The values of design points which have been considered herein all lie within the range of pilot's ratings considered good in Reference 3.

Figure 22 represents a dual Nyquist diagram which shows the effect of a change in desired short period damping-ratio. Three values of damping ratio are represented: $\zeta_1 = .45$, $\zeta_1 = .707$ and $\zeta_1 = 1.00$. The curves representing the loci of A(s) and the locus of -B(s) for $\zeta_1 = .707$ are identical to the curves in Figure 16. The curves in Figure 22 show that a change in desired damping ratio does not complicate the stability problem. The effect of a change in ζ_1 is so small as to be considered negligible.

An examination of Equation 47 reveals that the second term,

$$-\frac{2\zeta_1 s}{\omega_1\left(\frac{s}{\omega_{RG}}+1\right)}$$

is the only term in the expression for -B(s) which contains ζ_1. It can be shown by expressing the three terms of -B(s) as vectors and by computing their magnitudes and phase

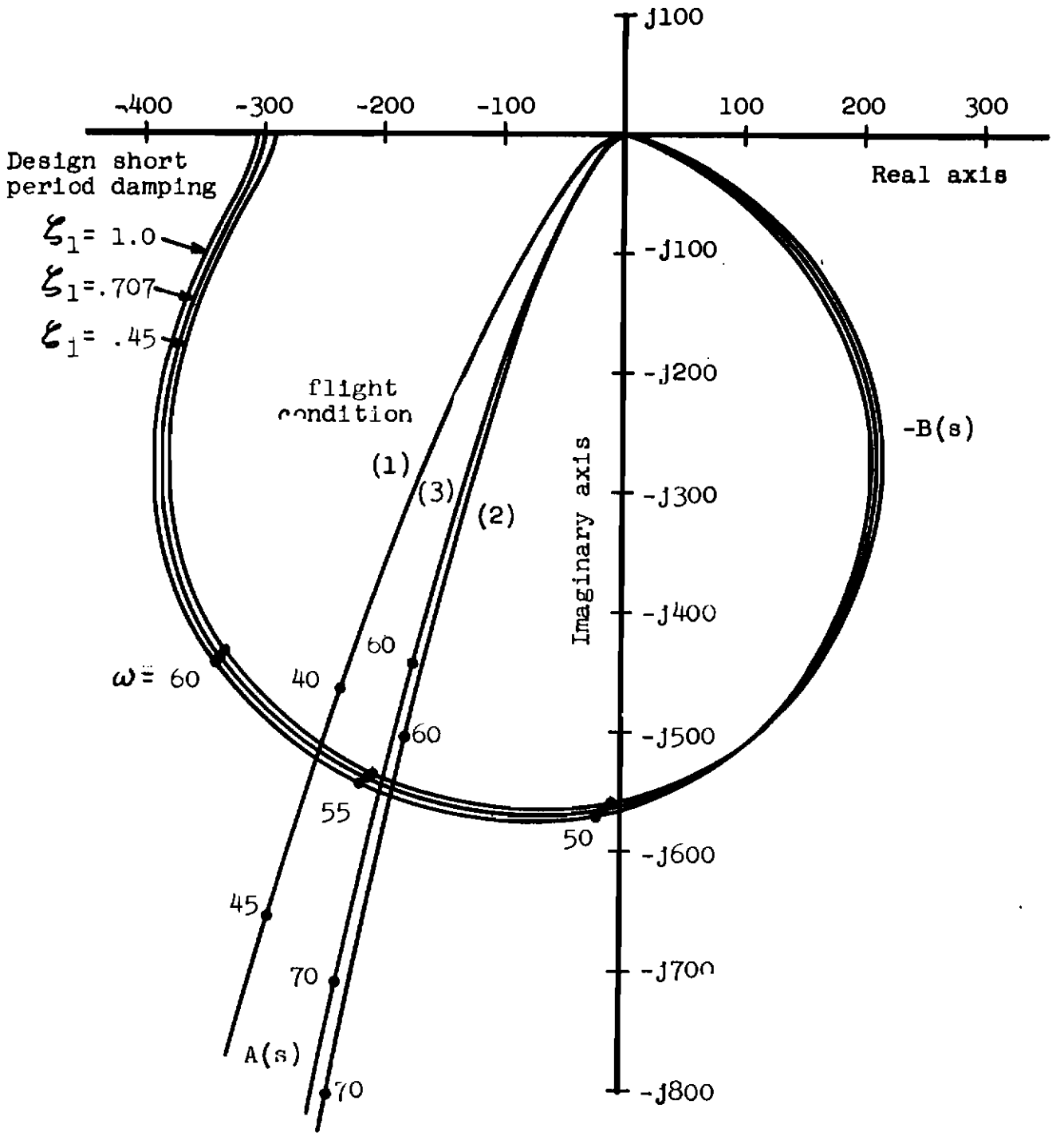

Fig. 22 DUAL NYQUIST DIAGRAM SHOWING EFFECT OF DESIGN SHORT PERIOD DAMPING-RATIO UPON STABILITY

angles that this second term contributes a nearly negligible magnitude to the total vector at high frequencies (frequencies equal to and greater than ω_{RG}). Furthermore a change in ζ_1 has no effect on the phase angle of the second term of -B(s). An increase in design damping ratio merely causes the points on the locus of -B(s) to shift slightly, ostensibly towards a more negative real part of -B(s). For these reasons, variations in ζ_1, within the range of values considered herein, have a negligible effect on the system stability for a given flight condition, loop gain, and particular servo and sensing instrument dynamics.

Effect of Design Short Period Natural Frequency Upon System Stability - Figure 23 represents a dual Nyquist diagram showing the effects of a change in desired short period natural frequency, ω_1. Three values are represented: $\omega_1 = 2$ radians per second, $\omega_1 = 3$ radians per second, and $\omega_1 = 4$ radians per second. The curves in Figure 23 indicate that an increase in ω_1 causes the locus of -B(s) to shrink radially towards the origin. This shrinking implies an increase in stability since the locus of B(s) will cross the locus of A(s) at a lower frequency on A(s). Therefore, the higher the desired short period frequency is made, the more stable the system becomes.

It has been shown previously that B(s) may be approximated by Equation 52. This approximation may be further simplified when it is applied to represent the loci of B(s) at the points of intersection with the loci of -A(s) in Figure 23. The loci of A(s) cross the loci of -B(s) at frequencies that are greater than ω_A. Since ω_A is much greater than ω_1, it follows that, at frequencies greater than or equal to ω_A, Equation 52 may be reduced to

$$B(s) \approx \frac{\frac{s^2}{\omega_1^2}}{\frac{s^2}{\omega_A^2} + \frac{2\zeta_A s}{\omega_A} + 1} . \qquad (55)$$

It is evident from Equation 55 that the magnitude of B(s) at any frequency greater than ω_A decreases as ω_1 is increased while the phase angle of B(s) remains unchanged. It may be concluded that, at high frequencies (in the range of the point of intersection on the dual Nyquist diagrams), increasing the value of ω_1 affects the stability of the system in much the same manner as decreasing the loop gain by the second power.

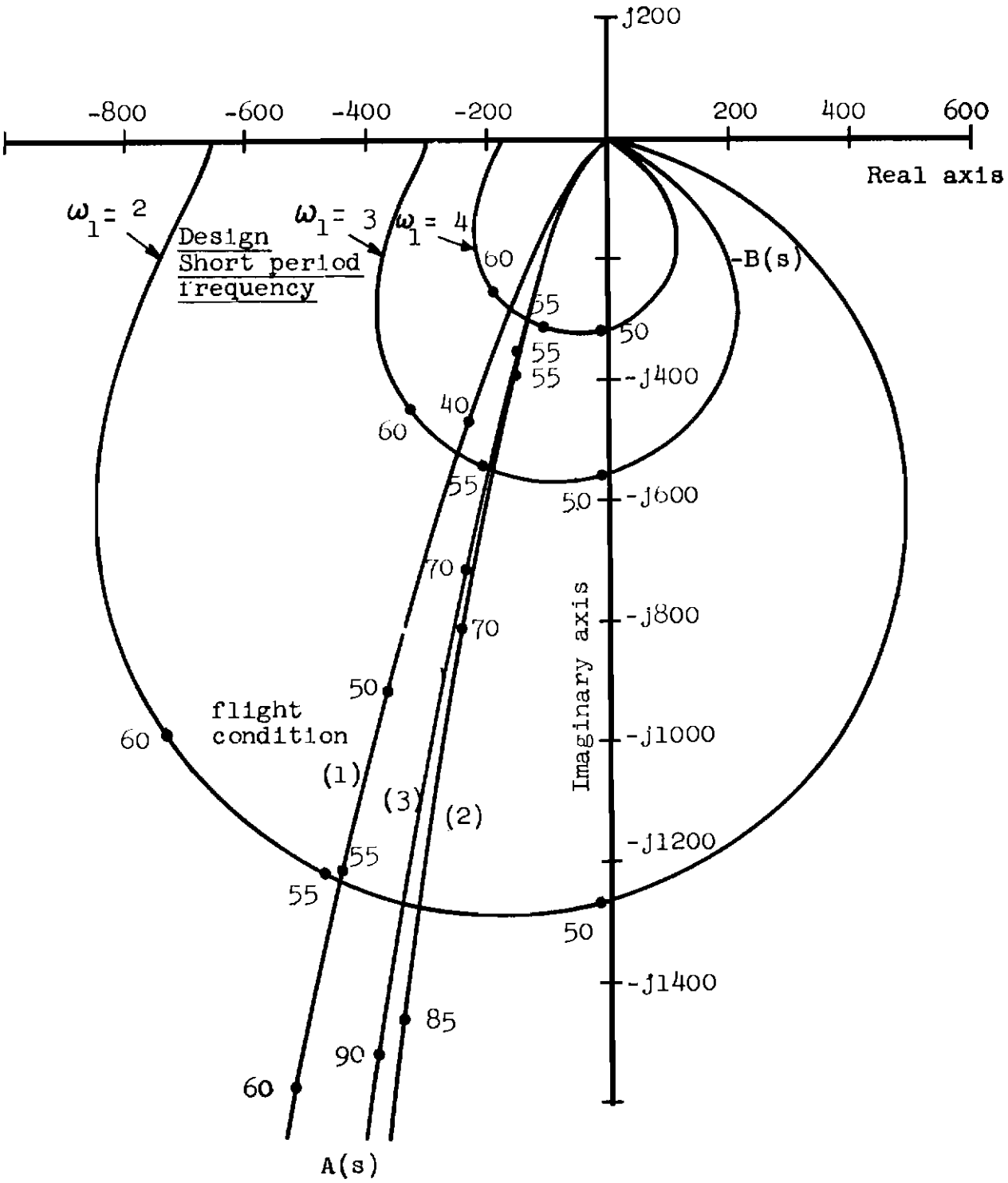

Fig. 23 DUAL NYQUIST DIAGRAM SHOWING EFFECT OF DESIGN SHORT PERIOD NATURAL FREQUENCY UPON STABILITY

Design Considerations in the Synthesis of the Final Control System

Selection of Servo Actuator and Sensing Element Characteristics - From the preceding discussion, several important conclusions may be drawn regarding the selection of servo actuator and sensing elements for the vehicle studied.

A hydraulic servo with the lowest characteristic frequency of those considered, 20 radians per second, appeared to result in the highest stability.

The rate gyro characteristic frequency could be selected arbitrarily within the range of frequencies which were examined (40 radians per second or greater). However, based on cost, the lowest characteristic frequency would appear to be the best choice.

An angular accelerometer with as high a natural frequency as is possible to achieve appears to be the most desirable. Although commercial angular accelerometers are available with natural frequencies as high as 600 radians per second, consideration was given herein to natural frequencies only as high as 250 radians per second. It will be shown in the discussion following that this value is quite adequate.

The larger the damping ratio of the accelerometer, the greater the stability gain margin. However, as will be seen, the dynamic effect of a large damping ratio must be given some consideration; this effect somewhat limits the selection of accelerometer damping ratio. The dynamic effect of damping ratio will be considered in the following discussion.

Considerations of Accelerometer Damping Ratio - In the final selection of the accelerometer damping ratio, consideration should be given to the effects of this parameter on system dynamic characteristics other than those of the short period. The closed loop transfer function, Equation 23,

may be written:

$$\frac{\theta_0(s)}{\theta_C(s)} = \frac{K_o K_2 \left(\frac{s}{\omega_{RG}} + 1\right)\left(\frac{s^2}{\omega_A^2} + \frac{2\zeta_A s}{\omega_A} + 1\right)}{\left(\frac{s}{\omega_{HS}} + 1\right)\left(\frac{s}{\omega_{RG}} + 1\right)\left(\frac{s^2}{\omega_A^2} + \frac{2\zeta_A s}{\omega_A} + 1\right)\left(\frac{s^2}{\omega_0^2} + \frac{2\zeta_0 s}{\omega_o} + 1\right) + \cdots}$$

$$\cdots + \frac{K_o K_2}{K_1}\left[\frac{s^2}{\omega_1^2}\left(\frac{s}{\omega_{RG}} + 1\right) + \frac{2\zeta_1 s}{\omega_1}\left(\frac{s^2}{\omega_A^2} + \frac{2\zeta_A s}{\omega_A} + 1\right) + \left(\frac{s}{\omega_{RG}} + 1\right)\left(\frac{s^2}{\omega_A^2} + \frac{2\zeta_A s}{\omega_A} + 1\right)\right] \qquad (56)$$

It can be shown that the denominator of Equation 56 has six roots which, for the parameters selected, consist of the short period complex conjugate pair, two negative real roots, and a pair of complex conjugates whose frequency is in the order of 200 radians per second and whose damping ratio varies from 0.1 to 0.4, depending upon the loop gain of the system. In all cases one of the negative real roots is almost exactly cancelled by the root $S = \omega_{RG}$ of the numerator of Equation 56. The other real root is of considerably larger magnitude and may therefore be considered negligible. If an accelerometer damping ratio of 0.25 is selected, the high frequency pair of complex conjugate roots of the denominator is approximately cancelled by the remaining roots of the numerator. Obviously, this cancellation effect diminishes as ζ_A is increased.

For the above reasons, it follows that, with a highly damped accelerometer ($\zeta_A = 2.0$), there will appear a high frequency, lightly damped oscillation in the system when the loop gain is set for a 3db gain margin. A lightly damped accelerometer ($\zeta_A = 0.25$) will essentially cancel out this high frequency oscillation; but, as was shown previously by dual Nyquist diagrams, the system gain margin (for a given loop gain) is decreased as ζ_A is decreased.

The above discussion serves to show that selection of accelerometer characteristics based entirely on obtaining the highest gain margin, for a given loop gain, does not necessarily produce the most desirable closed loop dynamic characteristics. The magnitude of the high frequency oscillation mentioned above increases with ζ_A. However, since ω_A is much greater than ω_1, the magnitude of this oscillation is necessarily small in comparison to that of the short period oscillation. Before selecting an accelerometer damping ratio, the designer must determine the amount of this high frequency oscillation, superimposed upon the short period motion, which can be tolerated.

Selection of Design Short Period Undamped Natural Frequency - There exist many factors such as resonances resulting from structural flexibility, maneuverability requirements, and handling qualities (if the vehicle is manned) which influence the choice of design short period undamped natural frequency. The above factors should be given primary consideration in any new application. In addition to these factors there is considerable merit in choosing the design frequency near the middle of the free airframe frequency range. When this is possible, it is evident that approximately the same degree of compensation is feasible at all flight conditions. On the other hand, the design frequency should be selected to be as large as possible within the limitations of the above considerations because stability margin increases with design frequency. The higher ω_1 is set, the more loop gain can be tolerated and the closer the design frequency can actually be approached. A reasonable compromise among all of these factors can probably be attained for most applications.

Pilots have expressed the opinion that a design short period natural frequency of 3 radians per second seems desirable (Reference 3). In addition, the natural frequencies of the free airframe discussed herein appear evenly distributed about this value. For these reasons a frequency of $\omega_1 = 3$ radians per second was selected.

Selection of Design Short Period Damping Ratio - It has been established that the design short period damping ratio is not influenced by stability considerations. A damping ratio of .707 is considered ideal in almost every application. The free airframe considered in this example is very deficient in damping with respect to the ideal. Therefore, at all flight conditions, the airframe with a self-adaptive control system will approach the ideal damping ratio from lower values of damping ratio. Since the difference between actual damping ratio and the design damping

ratio depends on the loop gain, the selection of ζ_1 depends upon the amount of gain that the system can tolerate. For this reason, it may be desirable to select a design damping ratio, ζ_1, that is larger than 0.707 so that the closed loop damping ratios will be distributed about 0.707. It will be assumed herein, that a closed loop damping ratio less than 0.707 and greater than some other value (.45 is a realistic minimum according to Reference 3) gives the system acceptable performance characteristics. For this reason, a design damping ratio of exactly 0.707 was selected.

Estimate of Short Period Characteristics of Final System - After component hardware dynamics and design short period characteristics have been selected on the basis of stability considerations and other related factors, the next step is to examine the deviations occurring in the closed-loop, short period root loci resulting from the inclusion of component dynamics. For the component dynamics which are being considered in the final system selection, reference to Figures 9, 10, and 11 indicates that the deviation of the root loci from the ideal is small enough for computing a first approximation of the closed loop damping ratio, natural frequency, and steady state gain by using Equations 11, 12, and 13.

The results of using the above component frequencies and of letting $\omega_1 = 3$ radians per second and $\zeta_1 = .707$ are shown in Table II. There are three sets of results listed representing three different choices of accelerometer damping ratio ($\zeta_A = 0.25$, 0.6 and 0.707). Shown are the closed-loop characteristics calculated from Equations 11, 12, and 13 for the three flight conditions previously defined.

Figure 24 is a graph of the results presented in Table II. The points represent the characteristics that are obtained for loop gains which produce a gain margin of 3 db at flight condition (3). It follows, then, that flight conditions (1) and (2) will have gain margins greater than 3 db. It is evident from this figure that all three values of accelerometer damping ratio give excellent results.

Considerations of Effects of Component Dynamics on Short Period Characteristics of Final System - The final system characteristics obtained in the preceding section are not difficult to calculate from Equation 9. This equation represents the transfer function of the closed-loop ideal system. By referring to Equation 23 or 56, it is seen that the exact characteristics are considerably more difficult to calculate since a sixth order polynomial must be factored. An estimate

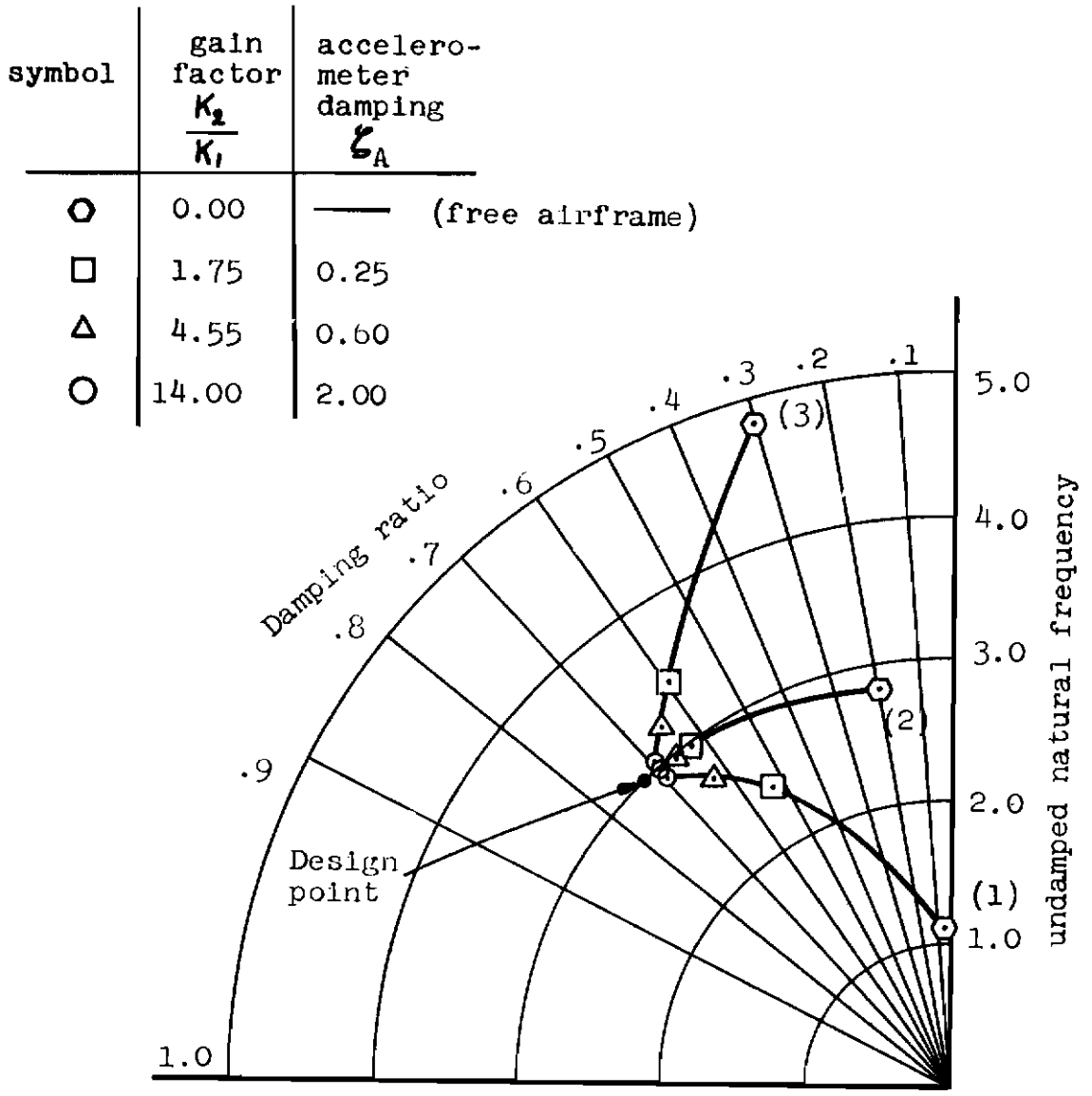

Fig. 24 APPROXIMATE CLOSED-LOOP, SHORT PERIOD CHARACTERISTICS AT A CONSTANT GAIN MARGIN FOR DIFFERENT ACCELEROMETER DAMPING-RATIOS

TABLE II

FIRST APPROXIMATION OF THE CLOSED-LOOP CHARACTERISTICS OF TYPICAL AIRFRAME WITH SELF-ADAPTIVE CONTROL

Gain Factor for 3db gain margin at condition (3) K_2/K_1	Accelerometer damping ζ_A	Closed-Loop Characteristics	Flight Conditions (1) $\omega_o = 1.1$, $\zeta_o = .05$, $K_o = 5.7$	Flight Conditions (2) $\omega_o = 2.8$, $\zeta_o = .2$, $K_o = 2.69$	Flight Conditions (3) $\omega_o = 4.84$, $\zeta_o = .3$, $K_o = 1.016$
1.75	0.25	K_3	.910 K_1	.825 K_1	.64 K_1
		ζ_3	.511	.614	.591
		ω_3	2.38	2.96	3.40
4.55	0.6	K_3	.963 K_1	.925 K_1	.822 K_1
		ζ_3	.615	.665	.653
		ω_3	2.69	2.99	3.18
14.0	2.0	K_3	.987 K_1	.975 K_1	.935 K_1
		ζ_3	.676	.694	.688
		ω_3	2.89	3.00	3.06

of the exact characteristics may, however, be obtained from a consideration of the effects of the component hardware dynamics upon the location of the short period roots. From previous discussion and the graphical results shown in Figures 9, 10, and 11, the following conclusions may be summarized in regard to a vehicle of the type studied.

1. As the hydraulic servo frequency decreases, the closed-loop roots shift from the ideal roots in a counterclockwise direction about the design point.

2. As the rate gyro frequency decreases, the real part of the roots shift farther into the left half plane.

3. The angular accelerometer natural frequency has little effect upon the roots if it is at least as great as 250 radians per second.

4. As the damping ratio of the accelerometer increases, the natural frequency associated with the roots decreases, but the damping ratio appears to remain essentially unchanged.

5. The above deviations of the roots from the ideal root locus are most pronounced in the midrange of values of loop gain.

By applying the above results to the root loci illustrated in Figure 24, the following deductions may be made regarding the exact closed-loop short period characteristic roots. For $\zeta_A = 0.25$, the roots will have a very slightly greater frequency and a more noticeably higher damping ratio than the ideal root because of effects (1) and (2) above. For $\zeta_A = 0.6$, the roots will again be higher in frequency and damping ratio than the ideal roots for the same reason, but the increase in frequency over the ideal will be less than for $\zeta_A = 0.25$ since effect (4) becomes more apparent, and the total shift will be less pronounced because of effect (5). For $\zeta_A = 2.0$, the total change from ideal to actual amounts essentially to an increase in damping ratio because the increase in frequency resulting from effects (1) and (2) is essentially cancelled by effect (4); again the deviation is considerably smaller than for the other two values of ζ_A resulting from effect (5).

In each of the preceding cases, the shift of the roots from their location with an ideal system is greatest for

flight condition (3) because in this condition the loop gain is the smallest of the three. By similar reasoning the smallest root shift occurs for condition (1).

Exact Short Period Characteristics of Final System - Factoring the denominator of Equation 56 was programmed for digital computer solution for each flight condition and three values of accelerometer damping. The final closed-loop short period roots are listed in Table III and illustrated graphically in Figure 25. A comparison of Figures 24 and 25 reveals that the inclusion of sensor and servo-actuator dynamics in the calculation of short period characteristics has actually produced desirable results in spite of the gain limitations imposed thereby. This improvement has been effected because all of the flight conditions shown represent cases where the free airframe is originally deficient in damping. Since the effect of the components is to shift the roots generally towards greater damping, an improvement should be expected for the conditions selected.

For the system illustrated in this report, the following component and design parameters appear to be optimum:

ω_1 = 3 radians per second

ζ_1 = 0.707

ω_{HS} = 20 radians per second

ω_{RG} = 40 radians per second

ω_A = 250 radians per second

ζ_A = 0.6

$\frac{K_2}{K_1}$ = 4.55

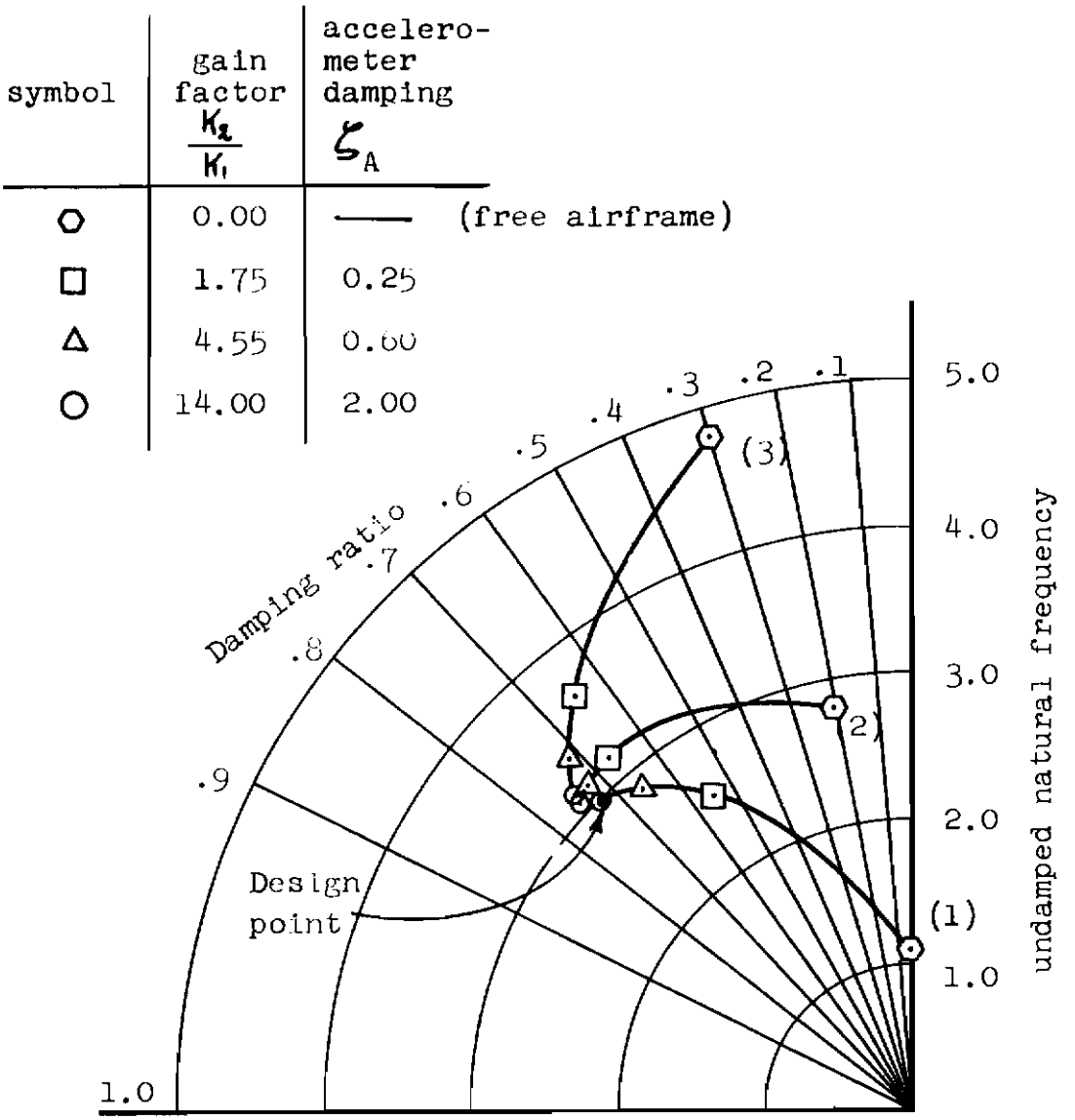

Fig. 25 EXACT CLOSED-LOOP, SHORT PERIOD CHARACTERISTICS AT A CONSTANT GAIN MARGIN FOR DIFFERENT ACCELEROMETER DAMPING-RATIOS

TABLE III

EXACT CLOSED-LOOP CHARACTERISTICS OF TYPICAL AIRFRAME WITH SELF-ADAPTIVE CONTROL

Gain Factor 3db gain margin at condition (3) K_2/K_1	Accelerometer damping ζ_A	Closed Loop Characteristics	Flight Conditions (1) $K_o = 5.7$, $\omega_o = 1.1$, $\zeta_o = .05$	Flight Conditions (2) $K_o = 2.69$, $\omega_o = 2.8$, $\zeta_o = .2$	Flight Conditions (3) $K_o = 1.016$, $\omega_o = 4.84$, $\zeta_o = .3$
1.75	0.25	K_3	.910 K_1	.825 K_1	.64 K_1
		ζ_3	.529	.648	.623
		ω_3	2.54	3.05	3.59
4.55	0.6	K_3	.963 K_1	.925 K_1	.822 K_1
		ζ_3	.642	.706	.697
		ω_3	2.87	3.15	3.34
14.0	2.0	K_3	.987 K_1	.975 K_1	.935 K_1
		ζ_3	.712	.733	.725
		ω_3	2.99	3.07	3.13

CONCLUDING REMARKS

A method of self-adaptive control has been shown to be feasible and applicable in a flight control system for the automatic stability augmentation of the short period response of a typical, powered, air-to-surface missile. The system comprises linear feedback of pitch attitude, pitch rate, and pitch angular acceleration with fixed gains. A second order representation of the airframe short period characteristic was assumed. Typical, present-day, stock control instrumentation (rate gyro, angular accelerometer, and hydraulic servo-actuator) was selected, and the dynamic characteristics of these components were included in the calculations. By using the above representation of the airframe, control instrumentation, and particular feedback arrangement, the following conclusions may be obtained:

1. Extreme feedback loop gains are not essential to reach near ideal short period characteristics at all flight conditions.

2. An adequate margin of stability can be maintained despite dynamic interaction of the control instrumentation with the control system.

3. The selection of sensing and actuating instrumentation is not critical, and it is only necessary to keep the following points in mind. The servo actuator must have a low characteristic frequency, preferably near 20 radians per second. The rate gyro dynamics (whether represented by first order characteristics or by second order characteristics) are not critical. The angular accelerometer should have a damping ratio near 0.6 and must have as high a natural frequency as possible although 250 radians per second appears to be adequate.

REFERENCES

1. Dandois, M., Concepts in Self-Adaptive Controls, Convair-Fort Worth Report FZA-270.

2. Heacock, R., Jones P., "Dual Nyquist Stability Analysis", Jet Propulsion Laboratory, California Institute of Technology, Pasadena, California, Memorandum No. 20-98.

3. Campbell, G., Use of an Adaptive Servo to Obtain Optimum Airplane Responses, Cornell Aeronautical Laboratory, Inc., Report No. C.A.L.-84.

APPENDIX A

THE THEORY OF THE DUAL NYQUIST CONCEPT

The dual Nyquist diagram is a graphical procedure for determining the stability of feedback systems. This procedure has advantages over the ordinary Nyquist diagram in certain cases. The dual Nyquist diagram may be used in all instances where the denominator of the transfer function of the system can be written as the sum of two frequency dependent functions.

A detailed discussion of this procedure is outlined in Reference 2. A short introduction to the method is given below.

To illustrate a point pertinent to the dual Nyquist concept, consider the simple feedback control system shown in Figure A-1.

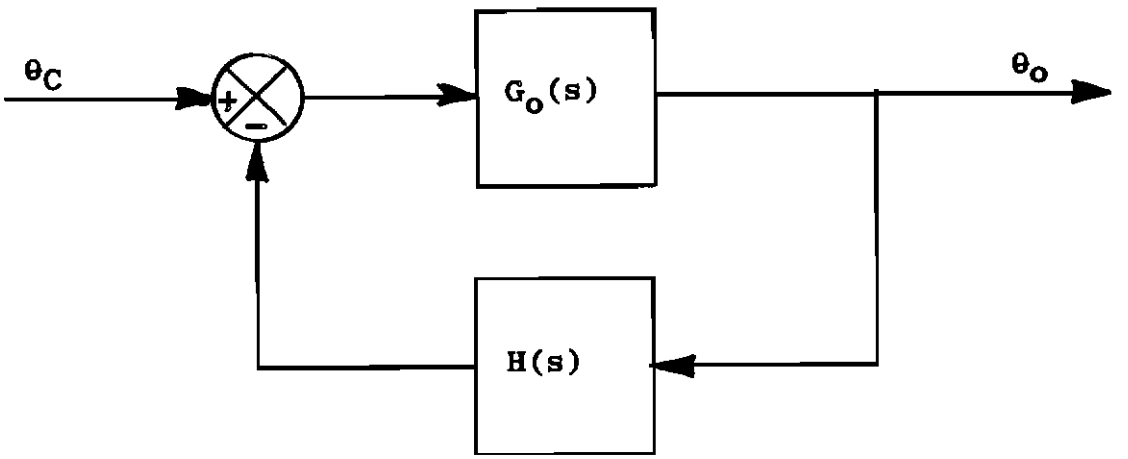

Fig. A-1 ILLUSTRATION OF SIMPLE FEEDBACK CONTROL

The closed-loop transfer function relating the output and input variables of this system is given by

$$\frac{\theta_0(s)}{\theta_C(s)} = \frac{G_0(s)}{1 + G_0(s)H(s)} \quad . \qquad \text{(A-1)}$$

The factor G(s)H(s) usually consists of a ratio, a sum or a product of frequency dependent functions, or some combination of these forms. By using several of these forms, the following examples can be utilized to illustrate the manner in which the denominator 1 + G(s)H(s) may be written as a sum of two frequency dependent functions.

$$\text{For} \quad G_o(s)H(s) = \frac{P(s)}{Q(s)} \; ; \quad \frac{\theta_0(s)}{\theta_C(s)} = \frac{G(s)Q(s)}{P(s) + Q(s)} \qquad \text{(A-2)}$$

$$\text{For} \quad G_o(s)H(s) = P(s)+Q(s); \frac{\theta_0(s)}{\theta_C(s)} = \frac{G(s)}{\left[1 + P(s)\right] + Q(s)} \qquad \text{(A-3)}$$

$$\text{For} \quad G_o(s)H(s) = P(s)Q(s); \frac{\theta_0(s)}{\theta_C(s)} = \frac{\frac{G(s)}{P(s)}}{\frac{1}{P(s)} + Q(s)} \cdot \qquad \text{(A-4)}$$

In any of the above cases, the denominator of the closed-loop transfer function assumes the form A(s) + B(s).

The ordinary Nyquist criterion in which the above form is used may be stated as follows: "The number of clockwise rotations of the vector $A(j\omega) + B(j\omega)$, on the complex plane, as the complex variable s traces a contour enclosing the positive real half of the complex plane but excluding singularities on the imaginary axis, plus the number of poles of G(s)H(s) with positive real parts must be zero for stability." For most systems, the condition of physical realizability (The function A(s) + B(s) must approach zero as s approaches infinity.) reduces the necessary plot of the s contour to that portion along the imaginary axis. In such systems the portion of the contour which is the infinite semicircle in the right half of the s plane maps into the origin of the A(s) + B(s) plane. In this discussion such a system has been assumed.

It must be understood, however, that certain algebraic manipulations of the transfer function, such as separating the denominator of the transfer function into the functions A(s) and B(s), may result in functions which no longer represent physical elements or loops of the system. In such cases, the functions A(s) or B(s) do not approach zero as s approaches infinity. Such a phenomenon is considered in the stability analysis of the airframe under examination in this report. The discussion which follows in this Appendix should therefore be extended to include the entire contour of s along the infinite semicircle in the right half plane in order to apply the dual Nyquist technique to any system of the type discussed in this report. Since the poles of G(s)H(s) are usually known in advance by inspection of the transfer functions of the forward path G(s) and the feedback path H(s), only the rotation of the vector $A(j\omega) + B(j\omega)$ need be determined. In the dual Nyquist diagram the locus of the vectors representing $A(j\omega)$ and $B(j\omega)$ are plotted separately. The information regarding the rotation of the sum of these two vectors is obtained by inspecting the points of intersection of the two loci.

To illustrate the general method, consider a closed-loop system whose transfer function is of the form

$$\frac{\theta_0}{\theta_C} = \frac{Fo(s)}{A(s) + B(s)} .$$

The following procedure is used. The function $F_1(j\omega)$ is plotted for values of ω from 0 to ∞. The function $-B(j\omega)$ is also plotted (Fig. A-2a). It is seen that if a vector is drawn from the $-B(j\omega)$ locus to the $A(j\omega)$ locus, with each end of the vector at the same value of ω, this vector will have the magnitude and direction of $A(j\omega) + B(j\omega)$. In this manner it is possible to visualize the locus of the function $A(j\omega) + B(j\omega)$ without carrying out the summation and plotting of the functions. It is also possible to determine the number of clockwise rotations of this vector by visualizing its successive angular positions as ω is varied from 0 to ∞.

Information regarding the stability of the system can be obtained more rapidly (without drawing the vector) by inspecting the points of intersection of the two loci. Figures A-2b and A-2c were drawn to illustrate the two basic ways in which two loci may intersect. In Figure A-2b the

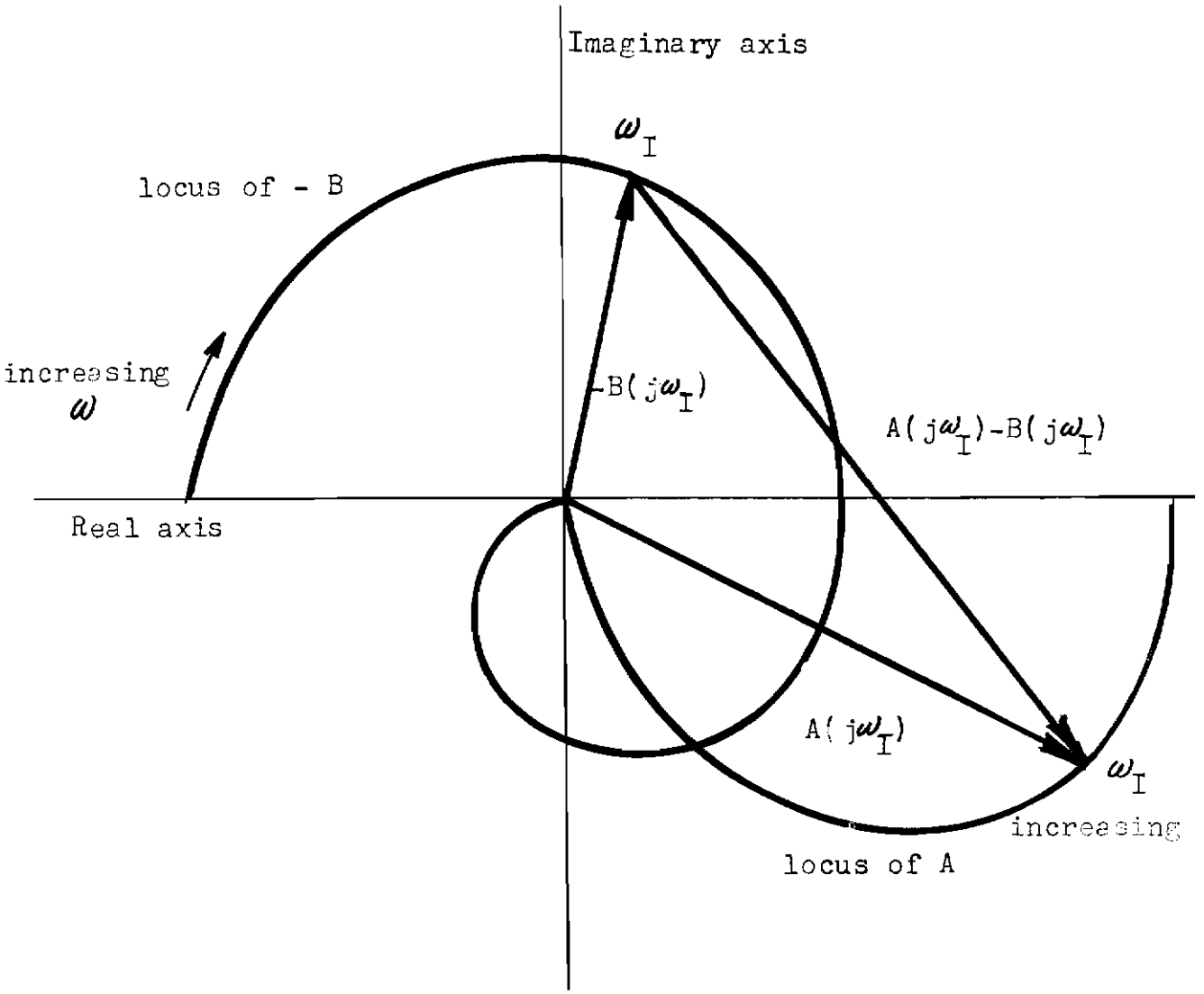

Fig. A-2a ILLUSTRATION OF DUAL NYQUIST DIAGRAM

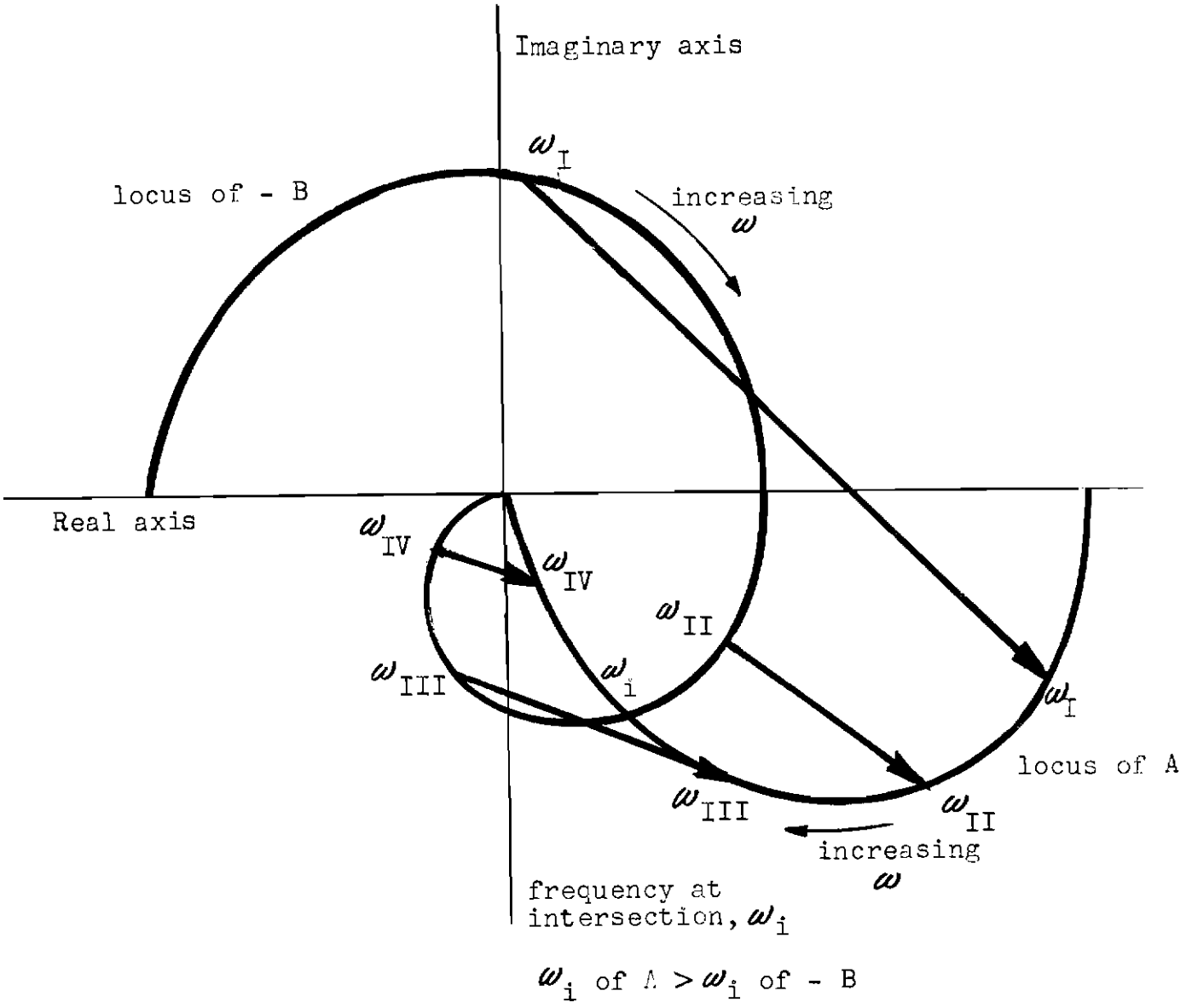

Fig. A-2b ILLUSTRATION OF DUAL NYQUIST DIAGRAM

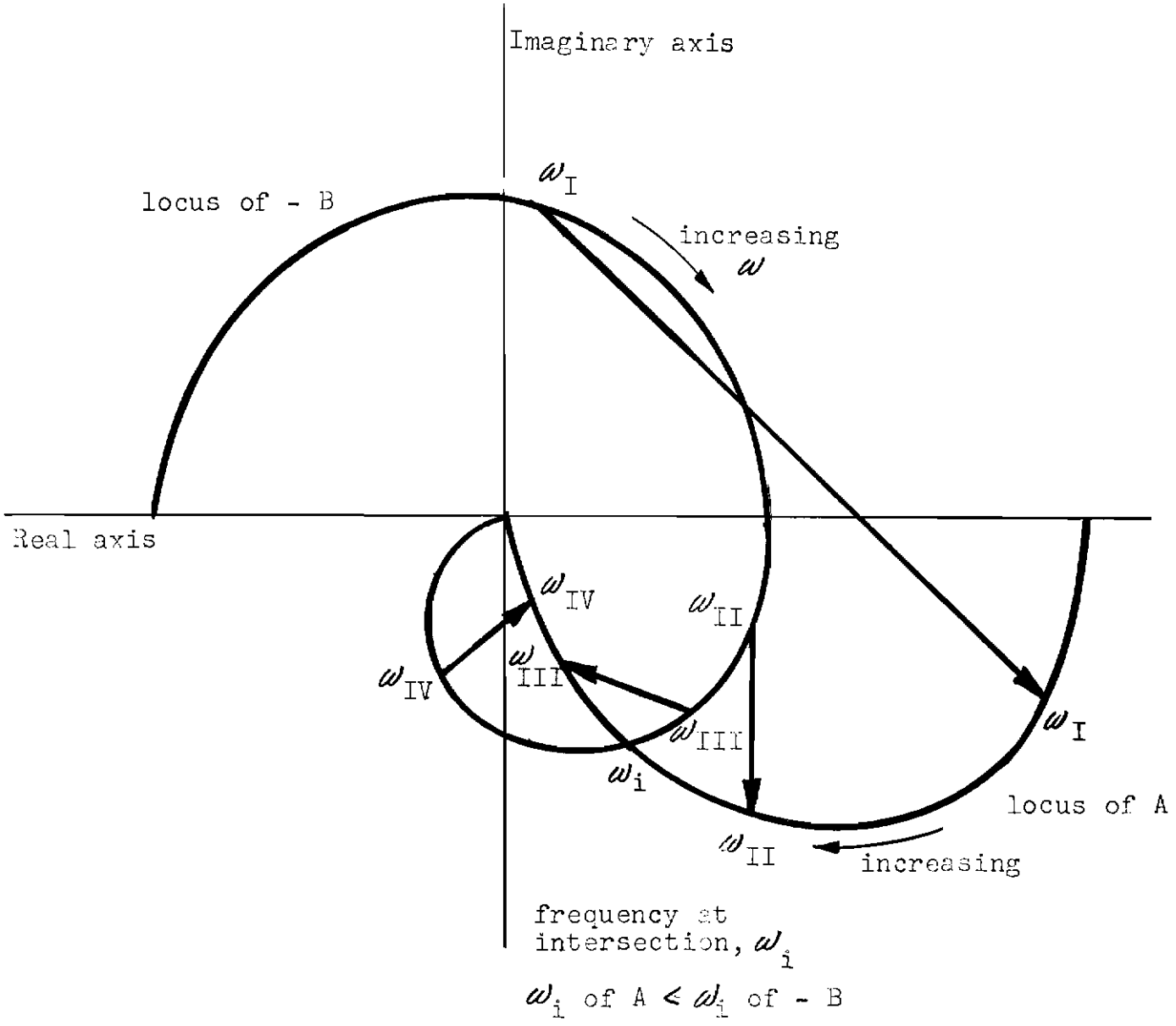

Fig. A-2c ILLUSTRATION OF DUAL NYQUIST DIAGRAM

locus of A enters the region enclosed by the locus of -B at a frequency which is greater than that of -B at the point of intersection. As a result it is seen that the vector $A(j\omega) + B(j\omega)$ makes zero net clockwise revolutions on the complex plane as ω varies from 0 to ∞. In Figure A-2c, on the other hand, the locus of A enters the region enclosed by the locus of -B at a frequency which is less than that of -B at the point of intersection. As a result, the vector makes one full rotation clockwise as ω ranges from 0 to ∞.

When the dual Nyquist diagram is plotted, it does not matter which of the functions, A or B, is plotted negatively. A general rule may be stated as follows: "Whenever one locus enters a region enclosed by the second locus at a lower frequency (or leaves at a higher frequency) than that existing on the second locus at the point of intersection, the vector $A(j\omega) + B(j\omega)$ makes one full clockwise rotation on the complex plane." The ordinary Nyquist criterion is then applied, as mentioned previously, by using the number of clockwise rotations obtained from the dual locus diagram.

Further remarks on the interpretation of the dual Nyquist diagram in various applications may be found in Reference 2. In applications to multiple loop systems, the dual Nyquist technique is especially useful since it allows the effects of a minor loop parameter to be obtained by plotting the Nyquist diagram of the characteristic equation of the minor loop as one of the two loci. Thus the stability of the inner loop may be obtained at the same time as the over-all stability is being determined. This procedure permits a more rapid determination of the effects of the inner loop parameters on the system stability.